

# Impact of Intravascular Hemolysis in Malaria on Liver Dysfunction

## INVOLVEMENT OF HEPATIC FREE HEME OVERLOAD, NF- $\kappa$ B ACTIVATION, AND NEUTROPHIL INFILTRATION\*

Received for publication, January 10, 2012, and in revised form, June 8, 2012. Published, JBC Papers in Press, June 13, 2012, DOI 10.1074/jbc.M112.341255

Sumanta Dey<sup>1</sup>, Samik Bindu, Manish Goyal, Chinmay Pal, Athar Alam, Mohd. Shameel Iqbal, Rahul Kumar, Souvik Sarkar, and Uday Bandyopadhyay<sup>2</sup>

From the Division of Infectious Diseases and Immunology, Council of Scientific and Industrial Research-Indian Institute of Chemical Biology, 4, Raja S. C. Mullick Road, Kolkata 700032, West Bengal, India

**Background:** Multiorgan failure is evident in conditions of intravascular hemolysis.

**Results:** Persistent intravascular hemolysis in malaria causes liver damage because of excess hepatic free heme accumulation, TNF $\alpha$  release, NF- $\kappa$ B activation, and neutrophil infiltration.

**Conclusion:** Intravascular hemolysis may result in hepatic failure as result of oxidative stress.

**Significance:** Intravascular hemolysis in any condition may damage liver or other vascular organs.

We have investigated the impact of persistent intravascular hemolysis on liver dysfunction using the mouse malaria model. Intravascular hemolysis showed a positive correlation with liver damage along with the increased accumulation of free heme and reactive oxidants in liver. Hepatocytes overinduced heme oxygenase-1 (HO-1) to catabolize free heme in building up defense against this pro-oxidant milieu. However, in a condition of persistent free heme overload in malaria, the overactivity of HO-1 resulted in continuous transient generation of free iron to favor production of reactive oxidants as evident from 2',7'-dichlorofluorescein fluorescence studies. Electrophoretic mobility shift assay documented the activation of NF- $\kappa$ B, which in turn up-regulated intercellular adhesion molecule 1 as evident from chromatin immunoprecipitation studies. NF- $\kappa$ B activation also induced vascular cell adhesion molecule 1, keratinocyte chemoattractant, and macrophage inflammatory protein 2, which favored neutrophil extravasation and adhesion in liver. The infiltration of neutrophils correlated positively with the severity of hemolysis, and neutrophil depletion significantly prevented liver damage. The data further documented the elevation of serum TNF $\alpha$  in infected mice, and the treatment of anti-TNF $\alpha$  antibodies also significantly prevented neutrophil infiltration and liver injury. Deferoxamine, which chelates iron, interacts with free heme and bears antioxidant properties that prevented oxidative stress, NF- $\kappa$ B activation, neutrophil infiltration, hepatocyte apoptosis, and liver damage. Furthermore, the administration of *N*-acetylcysteine also prevented NF- $\kappa$ B activation, neutrophil infiltration, hepatocyte apoptosis, and liver damage. Thus, hepatic free heme accumulation, TNF $\alpha$  release, oxidative stress, and NF- $\kappa$ B activation established a link to favor neutrophil infiltration in inducing liver damage during hemolytic conditions in malaria.

Intravascular hemolysis is a common pathological condition in a wide variety of diseases, including malaria, paroxysmal nocturnal hemoglobinuria, thalassemia, and sickle cell anemia (1, 2). Irrespective of the cases, severe hemolysis leads to several systemic complications and severe organ damage (1, 3–5). Renal failure, liver damage, spleen enlargement, lung injury, vascular injury, and stroke are some of the major complications due to hemolysis (1, 3–5). Hemolysis leads to the release of free hemoglobin in plasma. Once outside the red blood cells, hemoglobin dissociates to  $\alpha\beta$  dimers, which are bound by haptoglobin and removed from the circulation (6). However, once hemolysis becomes severe, haptoglobin fails to scavenge all the extracellular hemoglobin (7). Free ferrous hemoglobin in the plasma gets oxidized to ferrihemoglobin, which dissociates to free heme and globin (7). Free heme is removed from the blood by the protein hemopexin (8, 9), which is taken up by the hepatocytes through receptor-mediated endocytosis. Hemopexin similarly fails to counter the condition when hemolysis is severe and persistent. Under such conditions, free heme concentration is increased in serum. Besides the hemopexin-mediated heme transport to liver, there can be other ways of heme entry inside the liver when the hemopexin is saturated. Extracellular free hemoglobin and free heme is very toxic due to their pro-oxidant nature (10–16). The heme iron reacts with endogenous H<sub>2</sub>O<sub>2</sub> via the Fenton reaction and Haber-Weiss reaction to produce oxygen free radicals. The hydrophobic nature of heme allows it to intercalate into cell membranes causing the oxidant-mediated killing of cells (15, 17). The damage to cells and tissue is further aggravated in the presence of H<sub>2</sub>O<sub>2</sub>, which causes the release of iron from heme (18). Once inside the tissue, toxicity of heme is counteracted by the combination of heme oxygenase-1 (HO-1)<sup>3</sup> and ferritin.

\* This work was supported by Suprainstitutional Project grants from the Council of Scientific and Industrial Research, New Delhi.

<sup>1</sup> Recipient of a senior research fellowship from the Council of Scientific and Industrial Research, New Delhi.

<sup>2</sup> To whom correspondence should be addressed. Tel.: 91-33-24733491; Fax: 91-33-24730284; E-mail: ubandyo\_1964@yahoo.com.

<sup>3</sup> The abbreviations used are: HO-1, heme oxygenase-1; DFO, deferoxamine mesylate; NAC, *N*-acetylcysteine; *Icam1*, intercellular adhesion molecule-1; *Vcam1*, vascular cell adhesion molecule; KC, keratinocyte chemoattractant; MIP-2, macrophage inflammatory protein 2; AST, aspartate transaminase; ALP, alkaline phosphatase; ALT, alanine transaminase; DCFDA, 2',7'-dichlorodihydrofluorescein diacetate; MPO, myeloperoxidase; TNB, 5-thio-2-nitrobenzoic acid; DTNB, 5,5'-dithiobis-2-nitrobenzoic acid; PMN, polymorphonuclear.

The action of HO-1 on heme results in the generation of equimolar concentration of iron, biliverdin, and CO (15). Once released, this iron is generally chelated by ferritin (19), although the limits of ferritin are not known in pathological conditions. However, in conditions of persistent hemolysis and continuous supply of heme, HO-1 is overinduced and generated huge quantities of free iron, which may cross the limit of its ferritin sequestration. This chaos or failure of the cytoprotective system leads to severe oxidative stress-mediated cell death through necrosis and apoptosis (15, 20, 21).

Malaria, one of the most devastating infectious diseases, is endemic in 91 countries. Around 40% of the world's population is at risk of acquiring this dreadful infection. Each year, there are 300–500 million cases of malaria and 1.5–2.7 million deaths due to malaria (22). Intravascular hemolysis is highly accelerated due to malaria infection (23–25). In the erythrocytic stage, the malaria parasites modify the erythrocytes (26) and degrade ~60–80% of the total RBC hemoglobin (27, 28). Severe organ damage has been reported due to malaria infection (15, 28–34). However, the mechanism of organ damage under hemolytic conditions is not yet clear. Here, we provide evidence that intravascular hemolysis in malaria damages liver as a result of increased accumulation of free heme and reactive oxidants in liver, which favor neutrophil infiltration. We demonstrated that heme overload and oxidative stress activated the transcriptional factor NF- $\kappa$ B, which in turn enhanced neutrophil infiltration and extravasation through the up-regulation of intercellular adhesion molecules and chemokines. Furthermore, the chelation of free iron, scavenging of reactive oxidants, and depletion of neutrophil significantly prevented liver damage during malaria in mice.

## EXPERIMENTAL PROCEDURES

*In Vivo Growth of Plasmodium yoelii*—*P. yoelii* (MDR strain) is grown *in vivo* in male BALB/c mice (20–25 g) by inoculation of infected blood as described (35, 36). Parasite burden in blood (% parasitemia) was monitored by preparing a thin smear of blood and subsequent Giemsa staining. All animals are maintained in the animal house, and procedures were conducted in accordance with the guidelines of the Institutional Animal Ethics Committee and Committee for the Purpose of Control and Supervision of Experiments on Animals.

*Soret Spectroscopy to Detect Released Hemoglobin/Heme in Serum Due to Hemolysis and Assay of Liver Enzymes in Serum*—Blood was collected by puncture of the heart from different groups of mice and put into a 1.5-ml microcentrifuge tube. Serum was separated by centrifugation at  $600 \times g$  for 5 min and kept at  $-20^{\circ}\text{C}$ . Serum of different groups of mice was diluted (1:100) in distilled water and was analyzed in a spectrophotometer to determine the release of hemoglobin or heme from the erythrocytes in the serum. Although most of the heme in serum probably comes from hemolysis, it could also come from other sources such as muscle cells and hepatocytes. Activity of liver enzymes and bilirubin in serum of mice was measured to assess liver function. Enzyme activities of alanine transaminase (ALT), aspartate transaminase (AST), and alkaline phosphatase (ALP) were measured. We also measured the total amount of bilirubin and conjugated or direct bilirubin in serum. All assays

were performed by using kits purchased from Randox Laboratories Ltd. (Ardmore, Antrim, UK). Manufacturers' instructions were strictly followed. These assays served as parameters to evaluate the extent of hemolysis and liver damage in mice.

*Quantitation of Heme*—Total heme or free heme was quantified in serum and liver homogenate by using Quantichrome heme assay kit (Bioassay Systems) according to the manufacturer's instructions.

*Assay of HO-1 Activity*—HO-1 (Hmox1) activity in liver homogenate was measured based on the amount of bilirubin formed in an assay system as described (37, 38). Liver excised from a mouse was homogenized in a homogenization buffer (Tris-HCl, pH 7.4, 5 ml/liter Triton X-100, and protease inhibitor mixture). Liver homogenates from different groups of mice were used for the assay. The assay mixture consisted of a 1:1 mixture of liver homogenate (200  $\mu\text{g}$  of protein) and assay buffer (0.8 mM NADPH, 2 mM glucose 6-phosphate, 0.2 units of glucose 6-phosphate dehydrogenase, 1 mM  $\text{MgCl}_2$ , 100 mM potassium phosphate buffer, 20  $\mu\text{M}$  hemin, and 2 mg of mouse liver cytosol as a source of biliverdin reductase). The final volume was made up to 1 ml. The mixture was incubated at  $37^{\circ}\text{C}$  for 1 h in the dark. Reactions were terminated by keeping the samples on ice for 5 min. The bilirubin formed was extracted in chloroform, and  $A_{464-530}$  was measured. The amount of bilirubin formed was calculated from its extinction coefficient (40 mm/liter/cm) (37). The HO-1 activity was expressed as nanomoles of bilirubin formed per mg of protein/h.

*RNA Isolation and RT-PCR*—TRIzol reagent was used to isolate RNA from the perfused tissue according to the manufacturer's instructions (Invitrogen). Total RNA (2  $\mu\text{g}$ ) was then reverse-transcribed using the RevertAid First Strand cDNA synthesis kit (Fermentas) according to the manufacturer's instructions. The cDNA obtained was diluted for PCRs. The primers were purchased from Integrated DNA Technologies Inc. (San Diego). The primers are given along with their product size in Table 1. The cycling conditions for PCR amplification were as follows: initial denaturation at  $95^{\circ}\text{C}$  for 30 s and 40 cycles of denaturation at  $95^{\circ}\text{C}$  for 30 s, annealing at  $55^{\circ}\text{C}$  for 30 s, and extension at  $72^{\circ}\text{C}$  for 60 s, respectively. The PCR products were detected with 1.5% agarose gel electrophoresis, and densitometric analysis of the bands allowed semi-quantification. The images were captured using Quantity One<sup>®</sup> software (Bio Rad).

*Western Immunoblotting*—Liver was perfused for a long time to remove all contaminations of blood cells after which the homogenates were prepared. The perfused liver from different groups of mice was homogenized in a glass homogenizer in buffer (140 mM NaCl, 10 mM EDTA, 10% glycerol, 20 mM Tris, pH 8.0, supplemented with 1% Nonidet P-40 as detergent, and 20,000 units/ml aprotinin, 200 mM PMSF). The samples were then subjected to centrifugation for 20 min at  $13,000 \times g$  at  $4^{\circ}\text{C}$ . The supernatant (liver tissue lysate 70  $\mu\text{g}$ ) was mixed with protein loading buffer (Fermentas) and boiled for 4 min. The proteins were separated in a 12% SDS-polyacrylamide gel at constant voltage (100 V). Proteins were then transferred to a nitrocellulose membrane in a transfer apparatus with a current intensity of 400 mA for 120 min in a 190 mM glycine, 20 mM Tris base buffer, pH 8.3. The membrane was incubated for 3 h in the

**TABLE 1**  
**Primers for RT-PCR**

Primers used in this study are tabulated by the product size. Details of the PCR conditions are described under "Experimental Procedures."

Genes	Forward primer (5'–3')	Reverse primer (5'–3')	Product size bp
<i>Icam1</i>	taagaggactcggatgg	tttcccagactctcacagc	347
<i>Vcam1</i>	ctccacaaggctcaagagg	acgtcagaacaaccgaatcc	308
<i>Cxcl1</i>	tgagctgcgctgtcagtgctc	agaagccagcgttcaccaga	260
<i>Cxcl2</i>	gctggccaccaaccaccagg	agcgaggcacatcaggtacg	357
<i>Hmox1</i>	gcactatgtaaagcgtctcc	gactctggtctttgtgttcc	353
<i>Fth1</i>	ctttgccaaatactttctcc	aaagagatattctgcatgc	361
<i>ActB</i>	gtcagaaggactcctatgtg	gctcgttgccaatagtgatg	618
<i>Icam1</i> promoter	gagagatgagagggggaagg	gatccgctgtgagaaagtcc	363

blocking buffer TBS (25 mM Tris, 150 mM NaCl, 2 mM KCl, pH 7.4) to which 5% nonfat dry milk had been added. The mixture was then quickly washed with the same buffer without milk. The membrane was incubated overnight in the last buffer with 0.2% bovine serum albumin (BSA) solution containing 1:1000 anti-HO-1 (Abcam), ferritin heavy chain (US Biological), anti-NF- $\kappa$ B p65, IKK $\beta$ , I $\kappa$ B- $\alpha$ , and  $\beta$ -actin (Santa Cruz Biotechnology) for separate experiments. The membrane was then washed well with TBS containing 0.1% Tween 20. The membrane was incubated for 2 h in the same buffer containing secondary antibody (1:1000 HRP-labeled anti-rabbit or -goat IgG). The membrane was washed well with the incubation buffer. The protein detection was performed with a standard Western blot detection system. Pre-stained standards were used as molecular weight markers and were run in parallel.

**Isolation of Hepatocytes from Liver and Preparation of Lysates**—Hepatocytes were isolated from liver after perfusion by a two-step collagenase digestion method and purified by Percoll gradient (39). Hepatocytes were then counted and used for further experiments. For the preparation of hepatocyte lysates, cells were lysed in 100  $\mu$ l of buffer (140 mM NaCl, 10 mM EDTA, 10% glycerol, 20 mM Tris, pH 8.0, supplemented with 1% Nonidet P-40 as detergent, and 20,000 units/ml aprotinin, 200 mM PMSF) by three freeze-thaw cycles and sonication, and the cytosolic fraction was prepared by centrifugation at 13,000  $\times$  g for 20 min at 4  $^{\circ}$ C. Protein content in supernatant was determined by the method of Lowry *et al.* (40). An equal amount of protein was used for Western immunoblotting (41).

**Measurement of Free Iron-mediated Formation of Reactive Oxidants**—Hepatocytes isolated from different groups of mice were loaded with DCFDA (10  $\mu$ M) (Molecular Probes, Eugene, OR) for 30 min in the dark. Images were captured on a fluorescence microscope using a green filter. Upon oxidation, DCFDA exhibited bright green fluorescence (excitation/emission maxima  $\sim$ 490/515 nm), which was viewed under Leica DM 2500 fluorescence microscope (Leica Microsystems, GmbH, Wetzlar, Germany) (42, 43).

**Preparation of Nuclear Extract**—Nuclear extract from liver tissue was prepared with the help of two nuclear extraction buffers: Buffer I (10 mM HEPES, 1.5 mM MgCl<sub>2</sub>, 10 mM KCl, and 0.5% Triton X-100) and Buffer II (1 M NaCl, 0.2 M EDTA, 20% glycerol and 0.5 mM DTT). Liver tissues from different groups of mice were minced in the presence of Buffer I and then homogenized. The sample was then centrifuged, and the cytosol was separated. The pellet was resuspended in a mixture of Buffers I and II (1:1). The samples were vigorously vortexed for

30 s, kept on ice for the next 30 min, and centrifuged at high speed at 4  $^{\circ}$ C. The supernatants obtained were nuclear extracts and were stored at  $-80^{\circ}$ C until use.

**Electrophoretic Mobility Shift Assay (EMSA)**—NF- $\kappa$ B double-stranded consensus oligonucleotides 5'-AGTTGAGGGG-ACTTTCAGGC-3' and 3'-TCAACTCCCCTGAAAGGG-TCCG-5' (44, 45) were used for EMSA. The probes were labeled at the 5' end with T4 polynucleotide kinase (Fermentas) and [ $\gamma$ -<sup>32</sup>P]ATP (PerkinElmer Life Sciences). Excess unreacted ATP was removed from the labeled probe by ethanol precipitation at  $-20^{\circ}$ C (overnight) and washing with 70% ethanol. Binding reaction was performed with 10  $\mu$ g of nuclear protein in 10  $\mu$ l of binding buffer (10 mM HEPES buffer, pH 7.6, 50 mM NaCl, 1 mM EDTA, 5 mM MgCl<sub>2</sub>, 0.1 mM dithiothreitol, 1 mg/ml BSA and 0.05% Triton X-100). Samples were incubated for 30 min on ice. Complexes were separated by 5% native PAGE. Gels were fixed in a solution containing 30% methanol and 10% glacial acetic acid and dried in gel drying equipment. Dried gels were visualized by autoradiography. Antibody supershift assay was performed by incubating the sample with polyclonal antibodies against the p65 subunit of NF- $\kappa$ B (Santa Cruz Biotechnology) for 30 min on ice before <sup>32</sup>P-labeled probe addition. A competitive assay was also done by incubating the sample with cold probe (100-fold excess) for 30 min on ice before adding <sup>32</sup>P-labeled probe. To analyze the results of EMSA, a densitometric quantification of each spot of film was performed.

**Chromatin Immunoprecipitation (ChIP)**—Liver from different groups of mice were slightly minced and washed in cold PBS. After removal of PBS, the tissues were fixed in 1% formaldehyde in PBS. Nucleus was isolated as mentioned previously. Chromatin was sheared by sonication (10 times for 10 s at one-fifth of maximum power), centrifuged, and diluted in dilution buffer (50 mM Tris, pH 8.0, 5 mM EDTA, 0.2 M NaCl, and 0.5% Nonidet P-40). Extracts were pre-cleared for 2 h with a nonspecific antibody bound to protein A-Sepharose. For immunoprecipitation, 5  $\mu$ l of anti-NF- $\kappa$ B p65 (Santa Cruz Biotechnology) was added to protein A-Sepharose and incubated for 3 h. The unbound antibodies were removed by washing. The blocking step was performed with herring sperm DNA, which was added to the anti-NF- $\kappa$ B-protein A-Sepharose complex. A brief washing was done after blocking. The pre-cleared liver lysates were added and left overnight at 4  $^{\circ}$ C. Immune complexes were collected with protein A-Sepharose after a series of washings as follows: once in washing buffer (20 mM Tris, pH 8.0, 0.1% SDS, 0.5 M NaCl, 2 mM EDTA, and 1% Nonidet P-40) and once in 0.5 M LiCl, followed by three washes with TE buffer. Immune com-

plexes were extracted three times with 100  $\mu\text{l}$  of extraction buffer (TE buffer containing 2% SDS). DNA cross-links were reverted by heating for 8 h at 65 °C. After proteinase K (100  $\mu\text{g}$  for 2 h) digestion, DNA was extracted with phenol/chloroform and precipitated in ethanol. PCR was done both with DNA isolated from an aliquot of the total nuclear extract (input) and DNA isolated from the immunoprecipitated complex. Mouse *Icam1* promoter-specific primers (given in Table 1) were used for PCR at optimal PCR conditions and annealing was at 59 °C for 30 s. The PCR products were then analyzed in a 1% agarose gel. Quantitation of precipitated DNA relative to input DNA was undertaken using Quantity One® software (Bio-Rad).

**Isolation of Neutrophil from Mouse Blood**—Neutrophils were isolated from mouse blood as described (46). Neutrophil was isolated from mouse blood using the Histopaque gradient technique with slight modifications. 5 ml of mouse blood was slowly layered onto an equal volume of Histopaque (1077 mg/ml) in a 15-ml tube. This results in the formation of a two-step gradient. Then the tube was centrifuged at  $400 \times g$  for 45 min in a swinging rotor. The upper phase was discarded, and 2 ml of 6% dextran solution ( $M_r$  250,000–500,000) was added. The volume was increased to 7 ml with phosphate-buffered solution and homogenized. The tube was then incubated at 37 °C for 20 min. The supernatant was then centrifuged at  $270 \times g$  for 10 min. To remove erythrocytes, the pellet was then suspended in 0.83% (w/v)  $\text{NH}_4\text{Cl}$  and kept for 5 min after which it was again centrifuged at  $480 \times g$  for 10 min. Finally, the cells were washed with Hanks' balanced salt solution by centrifugation at  $270 \times g$  for 8 min and suspended in 1 ml of HBSS with 0.1% gelatin.

**Neutrophil Adhesion Assay**—Neutrophil adhesion assay was performed as described by Wiemer *et al.* (47). This gives a quantitative measurement of the number of neutrophils that adhere to hepatocytes isolated from different groups of mice under similar conditions. First, neutrophils were labeled with calcein-AM (Invitrogen) in a medium containing 1.93  $\mu\text{M}$  of the cell-permeable fluorescent indicator, calcein-AM (Invitrogen), for 15 min at 37 °C and 7.5%  $\text{CO}_2$ . The excess fluorescent dye was removed by washing the neutrophils with PBS without  $\text{Ca}^{2+}/\text{Mg}^{2+}$ . Neutrophils were then diluted to a concentration of  $1 \times 10^6$  cells/ml in Dulbecco's phosphate-buffered saline (D-PBS) without  $\text{Ca}^{2+}/\text{Mg}^{2+}$  for the standard curve or in a medium for further experiments. Prior to this experiment, hepatocytes were isolated from different groups of mice. The live cells were counted after isolation and washed well. Then the plates were coated with equal number of live cells. Neutrophils were then allowed to adhere for 30 min on hepatocyte-coated black medium-binding 96-well plates. After 30 min of incubation of the hepatocytes with the neutrophils, unbound neutrophils were removed by washing. Measurement of fluorescence was done at an excitation/emission of 485/535 nm using a Hitachi F-2500 fluorescence spectrophotometer. All samples were run in triplicate. The number of neutrophils adhered were counted with the help of a standard curve.

**Neutrophil Migration Assay**—Neutrophil migration or chemotaxis toward homogenates of liver from different groups of mice was studied in a Transwell system (Corning, NY) using 5- $\mu\text{m}$  polycarbonate membrane (34). Livers from different groups of mice were weighed and homogenized in an equal

volume of PBS ( $\text{Ca}^{2+}/\text{Mg}^{2+}$ -free) and centrifuged to collect the cytosol. An equal volume of all samples was then loaded in the bottom wells. Neutrophils present in RPMI 1640 medium ( $5 \times 10^4/50 \mu\text{l}$ ) were added to the upper wells and incubated for 2 h at 37 °C under 5%  $\text{CO}_2$  atmosphere. The number of migrated neutrophils was counted on Neubauer chambers. As a positive control, 1 nM leukotriene  $\text{B}_4$  was taken in the bottom wells, and for negative control only PBS was used. The ratio of the migrated neutrophils in the presence of samples or leukotriene  $\text{B}_4$  and the number of neutrophils migrated only in presence of PBS ( $\text{Ca}^{2+}/\text{Mg}^{2+}$ -free) is referred to as chemotactic indices.

**Detection of Neutrophils, Immunohistochemistry for Neutrophil Infiltration, and Myeloperoxidase (MPO) Assay**—Neutrophil infiltration in the liver was detected with the help of immunohistological study using primary neutrophil marker antibody (NIMP-R14) (Santa Cruz Biotechnology) and measuring MPO chlorination activity. For immunohistological characterization, specimens of liver were fixed in neutral buffered formalin, embedded in paraffin, cut in a microtome to 3–5  $\mu\text{m}$  thickness, and affixed onto the slide. This was followed by deparaffinization in xylene, rehydration in graded ethanol, proteolytic antigen retrieval, washing in TBS plus Triton X-100 (0.025%), blocking with 1% BSA in TBS, treatment with primary neutrophil marker antibody (NIMP-R14), treatment with FITC-conjugated secondary anti-rat antibody, washed well, and counter-stained with the fluorescent nucleic acid stain, DAPI. The slides were viewed under  $\times 20$  objective of a Leica DM 2500 fluorescence microscope (Leica Microsystems, GmbH, Wetzlar, Germany).

The measurement of MPO-chlorinating activity was based on the chlorination of taurine with the  $\text{MPO}/\text{H}_2\text{O}_2/\text{Cl}^-$  system (48). Prior to the start, preparation of TNB from DTNB was done. The pH of a 2 mM DTNB solution was raised to 12 to prepare TNB. TNB concentration was detected spectrophotometrically at 412 nm (extinction coefficient was  $14,100 \text{ M}^{-1} \text{ cm}^{-1}$ ) (48). Livers excised from different groups of mice were homogenized in PBS, pH 7.4, and were centrifuged at  $10,000 \times g$  for 10 min, and the supernatant was discarded. The pellet was then dissolved in ice-cold solubilization buffer containing 0.5% hexadecyltrimethyl ammonium bromide in PBS, pH 7.4. The samples were then sonicated and freeze-thawed three times to ensure lyses. Samples were then centrifuged at  $12,000 \times g$  for 30 min at 4 °C, and the supernatant was used for this assay. The temperature of the water bath was fixed at 25 °C, and the tubes containing 880  $\mu\text{l}$  of PBS, pH 7.4, and 80- $\mu\text{l}$  tissue samples were incubated for 5 min in the water bath. Then 40  $\mu\text{l}$  of 2.5 mM  $\text{H}_2\text{O}_2$  was added and mixed well. The reaction was terminated after 30 min by adding 40  $\mu\text{l}$  of catalase, and 100  $\mu\text{l}$  of TNB was added to each well. Hypochlorous acid reacts with taurine to produce taurine chloramine, which then reacts with yellow TNB to produce colorless DTNB. The absorbance was measured at 412 nm after 20 min. The decrease in TNB concentration was proportional to the amount of MPO in the sample, and MPO activity was expressed as units/g wet liver. One unit is the amount of MPO that can produce 1.0 nmol of taurine chloramine, which in turn can oxidize 2.0 nmol of TNB to DTNB under the given assay conditions.

## Intravascular Hemolysis and Liver Damage

**Depletion of Neutrophils**—Neutrophil depletion was performed as described (49) in mice by intraperitoneal administration of 100  $\mu$ l of anti-PMN antibody (host species, rabbit) (Accurate Chemicals, Westbury, NY) diluted 10 times in normal saline to make a total volume of 1 ml from day 3 to day 7 postinfection. Equal amounts of normal serum from rabbit was administered in separate groups of control and malaria-infected mice.

**Estimation of TNF $\alpha$  in Serum and TNF $\alpha$  Neutralization**—TNF $\alpha$  was measured from the serum of mice using an ELISA assay kit (RayBiotech, Inc., Norcross, GA).

TNF $\alpha$  neutralization in mice was done by intraperitoneal administration of 200  $\mu$ g of anti-TNF $\alpha$  antibody (host species, hamster) (e-biosciences) from day 3 to day 7 postinfection (23). Neutralization of TNF $\alpha$  was confirmed by ELISA of serum samples. Equal amounts of normal serum from hamster were administered in separate groups of control and malaria-infected mice.

**Animal Treatment with Deferoxamine Mesylate (DFO) and N-Acetylcysteine (NAC)**—Male BALB/c mice (20–25 g) with infection on “day 0” were treated as “control” group. Infected mice attained a parasitemia of 30–35% on day 4 and a peak parasitemia of 65–70% on day 8. Infected mice were treated with DFO and NAC, purchased from Sigma from the 3rd day of infection until the 7th day of infection, and experiments were performed on day 8. These treated groups of mice are referred to as “day 8 + DFO”- and “day 8 + NAC”-treated groups. There were six animals in each group. The dose of DFO and NAC was selected after a series of studies, and the optimal doses were reported. DFO was administered two times per day at 300 mg/kg, and NAC was administered once a day at 250 mg/kg for 5 consecutive days. All the drugs were administered intraperitoneally in water.

**Measurement of Oxidative Stress in Liver**—Lipid peroxidation was monitored in tissue by measuring the formation of thiobarbituric acid-reactive substances. The thiobarbituric acid-reactive substance were measured as described before (50, 51). A 5% homogenate of liver of different groups of mice was prepared in ice-cold 0.9% saline. Then 1 ml of each homogenate was mixed with a 2-ml solution containing trichloroacetic acid/thiobarbituric acid (0.375% w/v, 15% w/v, respectively) in 0.25 N HCl and 0.01% butylated hydroxytoluene. This was subjected to heating in a boiling water bath for 15 min and cooled at room temperature. The supernatant obtained after centrifugation of these samples was used for the spectrophotometric measurement of thiobarbituric acid-reactive substance at 535 nm. Tetraethoxypropane was taken as standard.

Protein carbonyl, a marker for oxidative stress, was measured as described previously (52). The livers from different groups of mice were homogenized in 50 mM sodium phosphate buffer, pH 7.4, to obtain a 10% homogenate. The samples were then centrifuged at 600  $\times$  g for 10 min, and the proteins in the supernatants were precipitated with 5% trichloroacetic acid. To the precipitated proteins 0.5 ml of 10 mM 2,4-dinitrophenylhydrazine was added and kept for 1 h. Next, the proteins were precipitated with 10% trichloroacetic acid and washed three times with a solution of ethanol/ethyl acetate (1:1). The samples were then dissolved in 0.6 ml of a solution containing 6 M guanidine-

HCl in 20 mM potassium phosphate (pH 2.3 with trifluoroacetic acid). The samples were subjected to centrifugation, and the supernatant was used for spectrophotometric measurement of carbonyl content at 362 nm.

**Detection of Apoptosis, Caspase-3 Activity, and Terminal Deoxynucleotidyltransferase dUTP Nick End Labeling (TUNEL) Assay**—Caspase-3 activity assay in liver homogenate was determined with a commercially available kit (Sigma) (36, 53). The absorbance of *p*-nitroanilide released from caspase-3 specific substrate (Ac-DEVD-*p*-nitroanilide) was measured at 405 nm in a microtiter plate reader. Results of caspase-3 activity are expressed as picomoles/mg of protein/min. Mean values of triplicate measurements were presented. TUNEL assay was performed to detect hepatic DNA fragmentation characteristic of apoptosis in liver sections with the help of DeadEnd<sup>TM</sup> colorimetric TUNEL system (Promega, Madison, WI) (35, 54). Briefly, paraffin-embedded liver sections from different groups of mouse livers were deparaffinized and then washed with PBS. The instructions given in the technical bulletin were strictly followed. Finally, the tissue sections were mounted in 80% glycerol, and the slides were observed in a light microscope.

**Data Analysis**—Data from all experiments were expressed as means  $\pm$  S.E. Calculations of the levels of significance were based on unpaired Student's *t* test and one-way analysis of variance as applied. A *p* value less than 0.05 (*p* < 0.05) was taken as statistically significant.

## RESULTS

**Association of Hemolysis with Liver Damage in Malaria**—To measure the impact of hemolysis on liver damage in malaria, we inoculated parasite (*P. yoelii*)-infected RBC to develop infection in mice, and in this process the parasite will not infect liver. The extent of hemolysis was analyzed through Soret spectroscopy by measuring extracellular hemoglobin or free heme in serum on day 0 (<1% parasitemia), day 4 (30–35% parasitemia), and day 8 (65–70% parasitemia) of postinfection (Fig. 1A). The level of serum hemoglobin (absorbance at 412 nm) increased with the increase of parasite burden with time indicating a positive correlation between parasite burden and hemolysis. Oxidation of free hemoglobin in serum leads to the formation of free heme in serum (7). Therefore, we measured the level of free heme, a major hemoglobin degradation product in serum (Fig. 1B). Results indicated a steady increase of free heme in serum with the increase of parasite burden with time. Free heme concentration was  $\sim$ 16  $\mu$ M in serum collected from malaria-infected mice on day 8. The presence of both free heme and hemoglobin in serum is an indication of severe hemolysis in malaria-infected mice. We also observed increased levels of ALT, AST, and ALP in serum, which are cellular markers for hemolysis. A significant increase of the level of these enzymes was correlated well with the increase of parasitemia with time after infection (Fig. 1C). The levels of ALT, AST, and ALP increased by  $\sim$ 6-,  $\sim$ 4-, and  $\sim$ 3-fold in malaria-infected mice on day 8. The increased level of these marker enzymes in serum not only indicates hemolysis but also indicates liver injury. Therefore, we were interested to evaluate the status of liver function under this hemolytic condition. To resolve this issue, we measured the direct and total bilirubin, a better indicator of liver injury, under

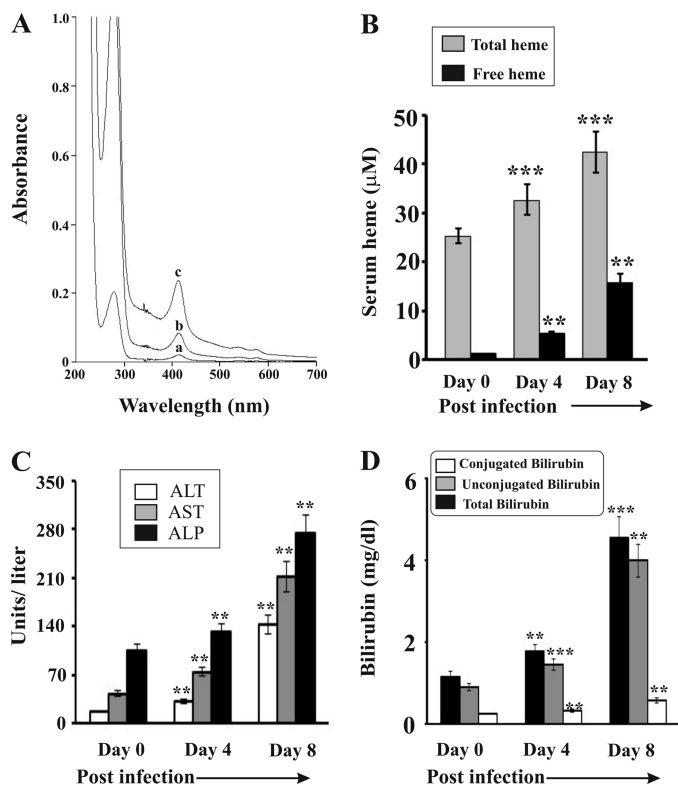


**FIGURE 1. Hemolysis and liver dysfunction in malaria-infected mice.** A, Soret spectroscopy of serum of malaria-infected mice on day 0 (a), day 4 (b), and day 8 (c) postinfection. B, measurement of heme in serum of malaria-infected mice on day 0, 4, and 8 postinfection. C, measurement of the activities of ALT, AST, and ALP in serum of malaria-infected mice on day 0, 4, and 8 postinfection. D, measurement of total, unconjugated, and conjugated bilirubin in serum of malaria-infected mice on day 0, 4, and 8 postinfection. Malaria-infected mice on day 0 is considered as control. The details of the methodology are described under "Experimental Procedures." Data are presented as mean  $\pm$  S.E. (\*\*,  $p < 0.01$  versus control; \*\*\*,  $p < 0.001$  versus control,  $n = 6$ ).

hemolytic conditions. We observed a significant increase in conjugated bilirubin (Fig. 1D) in serum of infected mice with the progress of infection indicating liver damage. It appeared that damage of the liver was positively associated with the severity of intravascular hemolysis as evident from the level of hemoglobin and free heme in serum in infected mice (Fig. 1).

**Evidence for Free Heme Overload and Reactive Oxidants in Liver of Infected Mice**—Hemolysis results in a high amount of free heme in blood, which is carried to the liver by hemopexin where the heme-hemopexin receptor on the hepatocyte membrane allows its entry inside the cells (8, 55). Under high hemolytic conditions, there are also other nonspecific ways for heme entry in the liver (56). Therefore, we quantified the amount of the total and free heme present in the liver in infected mice (Fig. 2A). The data indicate an increase of both total and free heme by 3-fold in the liver of mice on day 8 postinfection. Total heme takes into account both the heme present in all hemoproteins and the free heme in the liver. Overload of heme in the liver stimulated HO-1 activity significantly in malaria-infected mice with the increase of parasite burden (Fig. 2B). We also measured the expression of HO-1 and observed that both its transcript and protein levels were significantly elevated in infected mice as revealed by RT-PCR (Fig. 2C) and Western immunoblot (Fig. 2D) with the progress of infection. However, despite

overinduction of HO-1, free heme accumulated in the liver indicating that HO-1 could not act on all the heme molecules under acute hemolytic conditions. Heme, when degraded by HO-1, results in the formation of Fe(II). Free iron may also be produced due to the reaction of free heme with  $H_2O_2$ . The free iron produced was removed from the tissue by ferritin to neutralize its pro-oxidant effect. The expression of ferritin was also found to be augmented in the liver of infected mice as revealed by RT-PCR (Fig. 2C) and Western immunoblot (Fig. 2D). It is proposed that the continuous supply of free heme to the liver in malaria induced HO-1, which consequently produced a huge quantity of free iron by degrading free heme. Ferritin, however, was induced under these circumstances in the liver to sequester free iron but may have failed to prevent the immediate oxidative stress under severe conditions of infection.

Increased hepatic free heme may favor the generation of reactive oxidants because of their pro-oxidant nature. Heme may be degraded either by HO-1 or  $H_2O_2$ . This will result in the generation of free iron ( $Fe^{2+}$ ), and subsequently free iron may lead to the generation of oxidants. DCFDA (Molecular Probes, Invitrogen), a fluorescent redox indicator probe, was used to see the alterations in free iron signaling in hepatocytes isolated from the liver of infected mice (42). The data indicated a significant alteration in redox reactions mediated by free iron or the presence of one-electron-oxidizing species (green fluorescence), and it was found to be increased again with the progress of parasitemia with time (Fig. 3).

**NF- $\kappa$ B Overexpression and Activation in Liver during Malaria Infection**—Excessive alteration of redox reactions may be a cause of oxidative stress that can stimulate NF- $\kappa$ B in the liver of infected mice. NF- $\kappa$ B is a major transcription factor controlling a wide array of genes (57, 58). We were interested to find out the response of NF- $\kappa$ B in liver in hemolytic conditions. Activation of NF- $\kappa$ B under conditions of oxidative stress is dependent on its upstream proteins IKK $\beta$  and I $\kappa$ B. IKK $\beta$  stimulation or reactive oxidants stimulate I $\kappa$ B degradation, which activates NF- $\kappa$ B and allows it to translocate from the cytosol to the nucleus (59). We performed Western immunoblotting to determine the levels of IKK $\beta$ , I $\kappa$ B, and NF- $\kappa$ B in the liver of infected mice. The data indicated that the expression of IKK $\beta$  was induced with the increase of parasite burden with time (Fig. 4, A and B). Densitometric analyses revealed an  $\sim$ 3-fold increase in the expression of IKK $\beta$  in the liver of malaria-infected mice on day 3 and 5–6-fold increase in liver of malaria-infected mice on day 8 (Fig. 4B). We found an increase of I $\kappa$ B degradation in the liver of infected mice in parallel to the increase of IKK $\beta$  expression (Fig. 4, A and B). I $\kappa$ B degradation led to activation of NF- $\kappa$ B and its transport inside the nucleus as revealed by electrophoretic mobility shift assay (EMSA) (Fig. 4C). No detectable complex was formed when a protein of the nuclear extract obtained from mouse liver on day 0 postinfection was subjected to EMSA with an oligonucleotide probe containing the NF- $\kappa$ B-binding sequence (Fig. 4C, lane 1). In contrast, a clear shift of band was observed using nuclear extracts from the liver of infected mice on day 4 postin-

## Intravascular Hemolysis and Liver Damage

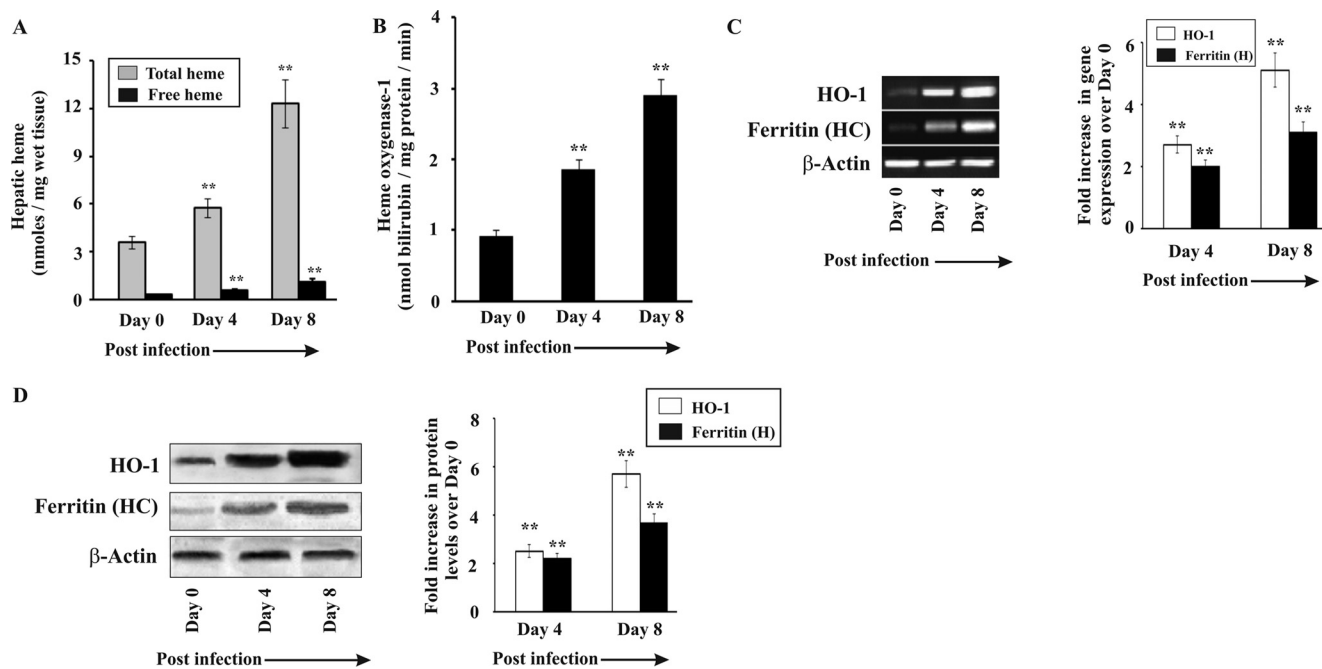


**FIGURE 2. Status of heme, heme oxygenase-1, and ferritin in liver of infected mice.** *A*, measurement of heme in liver of malaria-infected mice on day 0, 4, and 8 postinfection. *B*, heme oxygenase-1 activity in liver of malaria-infected mice on day 0, 4, and 8 postinfection. *C*, RT-PCR analysis of heme oxygenase-1 and ferritin (heavy chain) in liver of malaria-infected mice on day 0, 4, and 8 postinfection. *D*, Western immunoblot analysis of heme oxygenase-1 and ferritin (heavy chain) in liver of malaria-infected mice on day 0, 4, and 8 postinfection. Malaria-infected mice on day 0 is considered as control. The details of the methodology are described under "Experimental Procedures." Data are presented as mean  $\pm$  S.E. (\*,  $p < 0.1$  versus control; \*\*,  $p < 0.01$  versus control,  $n = 6$ ).

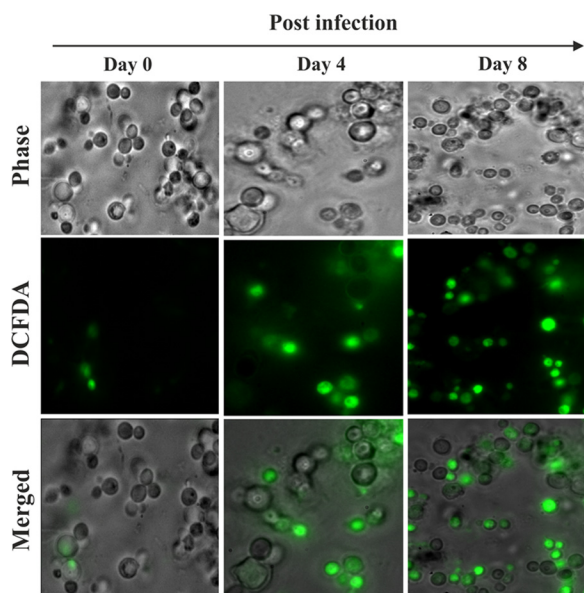


**FIGURE 3. Induction of iron-mediated reactive oxidant generation.** Iron-mediated reactive oxidant generation was measured in liver of malaria-infected mice on day 0, 4, and day 8 postinfection. Detection of reactive oxidants by DCFDA (green fluorescence) in hepatocytes isolated from the liver of infected mice. The details of the methodology are described under "Experimental Procedures."

fection, which increased significantly with time until day 8 (Fig. 4C, lanes 2 and 3) indicating the formation of NF- $\kappa$ B-DNA complex. The NF- $\kappa$ B-DNA complex formation was completely inhibited in the presence of an excess of unlabeled oligonucleotide probes indicating the specificity of binding (Fig. 4C, lane 4). No band was detected when a free labeled probe was run in absence of nuclear extract (Fig. 4C, lane 5). A distinct super-

shifted band was detected when the nuclear extracts of liver of severely infected mice were incubated with the NF- $\kappa$ B antibody (Fig. 4C, lane 6). Densitometric analyses of the NF- $\kappa$ B-DNA complex revealed  $\sim 1.7$ - and  $\sim 2.5$ -fold increase in day 4 and day 8 postinfected liver nuclear extracts (Fig. 4D). An increase in the NF- $\kappa$ B level in the nuclear extract was confirmed through immunoblotting and subsequent densitometric analysis. The data were normalized with the band obtained by using a control antibody against histone H3 (Fig. 4E).

We purified hepatocytes by Percoll gradient to demonstrate NF- $\kappa$ B activation in the hepatocyte. Cell lysates and nuclear extracts were prepared from these purified hepatocytes for Western immunoblotting. Data indicated that there was a significant increase in NF- $\kappa$ B levels both in the lysate and in the nuclear extracts indicating translocation of NF- $\kappa$ B in the nucleus (Fig. 4, F and G).

**Expression of Adhesion Molecules, Neutrophil Adhesion, and Chemotaxis in Liver of Infected Mice**—NF- $\kappa$ B activation leads to the induction of endothelial cell adhesion molecules and chemokines, which promote neutrophil infiltration and adhesion (58). RT-PCR data documented that adhesion molecules and chemokines were significantly induced in liver with the increase of parasitemia (Fig. 5A). The expressions of *Icam1*, *Vcam1*, *Cxcl1* (KC), and *Cxcl2* (MIP-2) were significantly high with the progress of infection with time (Fig. 5A). The fold increment of the expression was analyzed by densitometric analysis of the transcript of these genes with respect to the control (Fig. 5B). All the above mentioned genes have a  $\kappa$ B binding sequence in their promoters, and  $\kappa$ B binding results in the induction of expression of these genes. We performed a ChIP assay to check the binding of NF- $\kappa$ B to the promoter. We chose to study the binding of NF- $\kappa$ B to *Icam1* promoter, a rep-

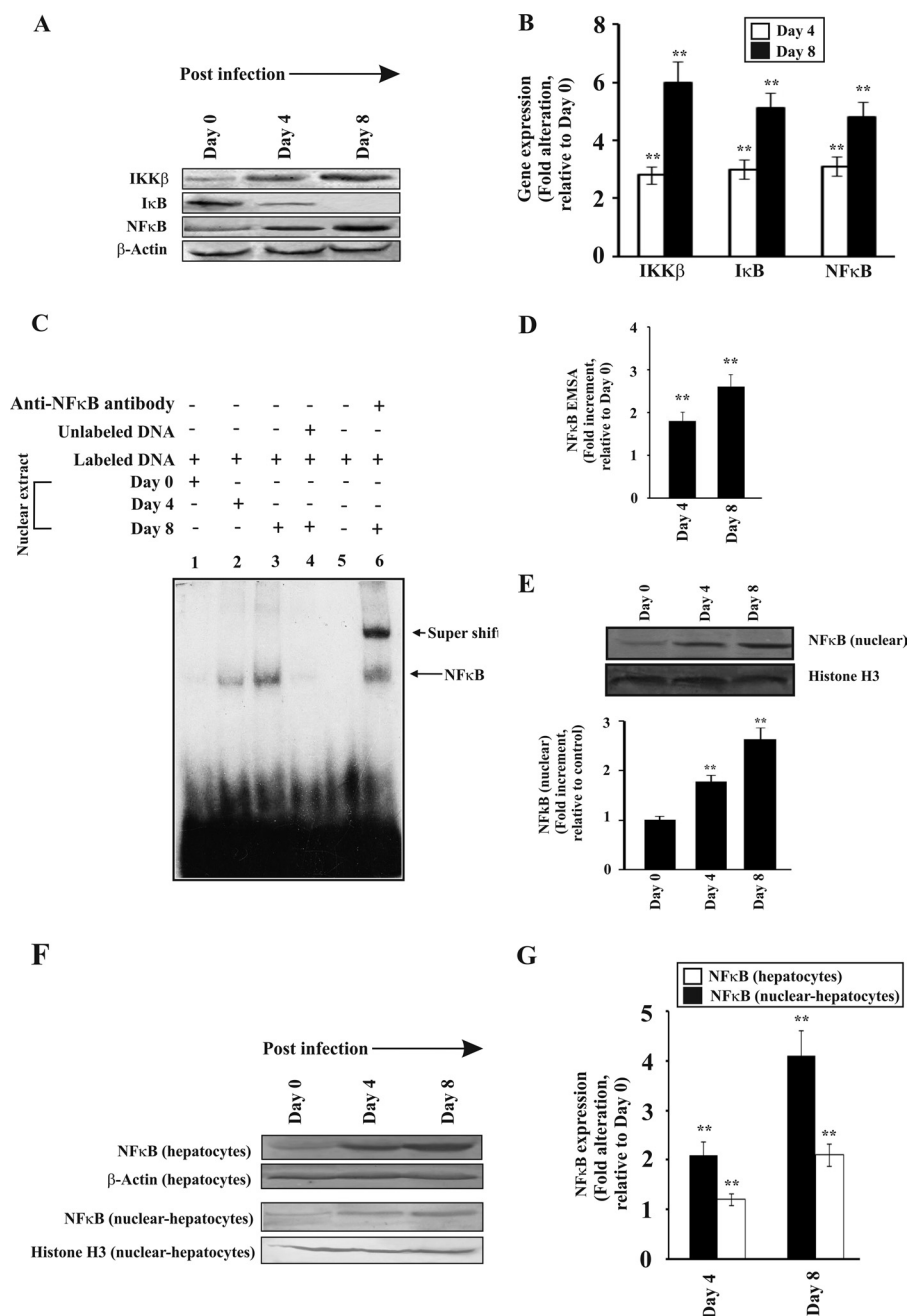


**FIGURE 4. Activation of NF- $\kappa$ B in the liver of malaria-infected mice.** NF- $\kappa$ B activation was monitored in three separate groups of mice on day 0, 4, and 8 postinfection. *A*, Western immunoblot of IKK $\beta$ , I $\kappa$ B, and NF- $\kappa$ B in liver homogenate of infected mice on different days after infection. *B*, assessment of the expression of IKK $\beta$ , I $\kappa$ B, and NF- $\kappa$ B by densitometric analyses of the Western immunoblot data. *C*, translocation of NF- $\kappa$ B to nucleus as documented by EMSA. Lane 1, nuclear extract of liver from mice on day 0 postinfection with labeled probe; lane 2, nuclear extract of liver from infected mice at day 4 postinfection with labeled probe; lane 3, nuclear extract of liver from infected mice at day 8 postinfection with labeled probe; lane 4, nuclear extract of liver from severely infected mice with labeled probe and competition with 100-fold excess of cold probe; lane 5, only labeled probe and no nuclear extract; lane 6, supershift with an antibody specific for NF- $\kappa$ B and nuclear extract of liver from infected mice on day 8 postinfection. *D*, densitometric analysis of EMSA. *E*, detection of NF- $\kappa$ B in nuclear extract from liver of different groups of infected mice by Western immunoblot and its densitometric analysis (lower panel). *F*, Western immunoblot of NF- $\kappa$ B in hepatocyte lysates and nuclear extracts isolated from hepatocytes of infected mice on different days postinfection.  $\beta$ -Actin and histone H3 served as loading controls for hepatocyte lysates and nuclear extracts, respectively. *G*, densitometric analyses of Western immunoblot. Malaria-infected mice on day 0 is considered as control. The details of the methodology are described under "Experimental Procedures." Data are presented as mean  $\pm$  S.E. (\*\*,  $p < 0.01$  versus control,  $n = 6$ ).

representative of the above mentioned genes. Isolated chromatin from days 0, 4, and 8 postinfected mice were immunoprecipitated by anti-NF- $\kappa$ B p65 antibody or rabbit IgG (as negative control). PCR analysis showed that NF- $\kappa$ B p65 antibody precipitated the *Icam1* promoter region from infected mice (Fig. 5C, top panel), whereas the same from control mice (day 0 infected)

did not demonstrate any significant DNA binding (Fig. 5C, top panel). Chromatin samples immunoprecipitated by rabbit IgG did not exhibit any DNA binding as revealed by PCR analysis (Fig. 5C, 2nd panel). Input samples confirmed equal loading of samples. Therefore, data revealed a steady increase in the binding of NF- $\kappa$ B to *Icam1* with increase in time after infection (Fig.

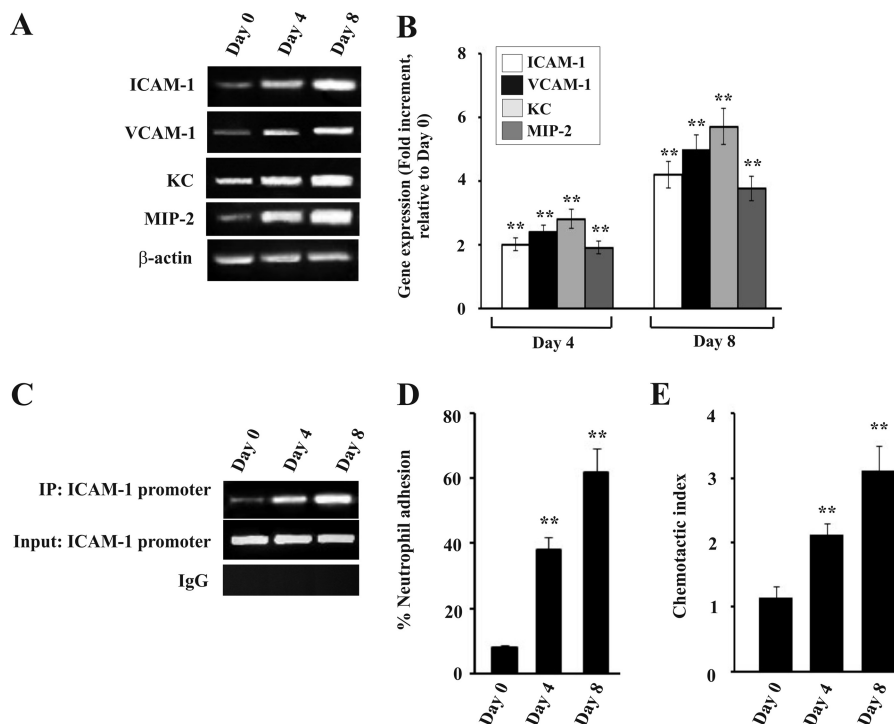


**FIGURE 5. Expression of endothelial cell adhesion molecules and neutrophil chemoattractants (CXC chemokines) in the liver of malaria-infected mice and measurement of neutrophil adhesion.** The expression of adhesion molecules and the neutrophil adhesion was checked in liver of three separate groups of mice on day 0, 4, and 8 postinfection. *A*, RT-PCR analysis of *Icam1*, *Vcam1*, *Cxcl1* (KC), *Cxcl2* (MIP-2), and *Actb* ( $\beta$ -actin). *B*, densitometric analyses of the RT-PCR data. *C*, ChIP analysis to follow the recruitment of NF- $\kappa$ B on *Icam1* gene promoter. *Lanes 1–3*, loaded with samples of infected mice on day 0, 4, and 8 postinfection. *Upper panel*, ChIP assay PCR products from immunoprecipitates obtained using antibodies against NF- $\kappa$ B with nuclear extracts of liver; *2nd panel*, input denotes amplification of the DNA in soluble chromatin before immunoprecipitation. *Bottom panel*, chromatin immunoprecipitated with normal rabbit IgG. *D*, neutrophil adhesion assay with liver cells isolated from infected mice on day 0, 4, and 8 postinfection. *E*, chemotactic index of neutrophils indicating neutrophil migration in liver of infected mice on day 0, 4, and 8 postinfection. Malaria-infected mice on day 0 is considered as control. The details of the methodology are described under “Experimental Procedures.” Data are presented as mean  $\pm$  S.E. (\*\*,  $p < 0.01$  versus control,  $n = 6$ ).

5C). Furthermore, to confirm the increase in endothelial cell adhesion molecules on the surface of hepatocytes, cells were isolated from the liver of infected mice. Incubation of calcein-labeled neutrophils with hepatocytes clearly indicated that adhesion of neutrophils to hepatocytes from infected mice significantly increased with time after infection as evident from fluorescence intensity. This increase in adhesion of neutrophils was positively correlated with parasite burden (Fig. 5D). Furthermore, we performed neutrophil chemotaxis assays to document neutrophil attraction toward the liver homogenate of mice, which was prepared after extensive perfusion of the tissue. The chemotaxis of neutrophil was represented as chemotactic index, and it was positively correlated with the increase of parasite burden and hemolysis (Fig. 5E).

**Evidence for Neutrophil Infiltration in Liver and Its Effect on Liver Damage during Malaria**—The data indicated a significant infiltration of neutrophils in liver sinusoids and extravasation inside the liver parenchyma cells during malaria in mice (Fig. 6). The presence of neutrophils in liver was assessed by immunofluorescence studies with neutrophil marker antibody (Fig. 6, A and B). In the liver of infected mice on day 0, insignificant infiltration of neutrophils was evident (Fig. 6, A and B). However, neutrophil infiltration was found to be prominent and increased gradually with the severity of parasitemia. In the liver of infected mice on day 4 postinfection, the number of neutrophils (as indicated by green fluorescence of neutrophil-bound neutrophil marker (NIMP-R14) antibodies) in the

sinusoids and parenchyma was comparatively less than in the liver of mice on day 8 postinfection (Fig. 6, A and B). MPO activity in the liver of infected mice was measured for further confirmation of neutrophil infiltration. MPO chlorination activity was found to be increased with the increase of parasite burden and hemolysis (Fig. 6C).

We used an anti-PMN antibody to deplete neutrophils in mice to confirm the role of neutrophils in liver damage in malaria. Depletion of neutrophils was carried out by administration of anti-PMN antibody daily from day 3 to day 7. Neutrophil depletion prevented oxidative stress as evident from reduced lipid peroxide and protein carbonyl formation (Fig. 6D). Neutrophil depletion also inhibited the induction of apoptosis as evident from caspase-3 activity assay (Fig. 6E). Subsequently, neutrophil depletion in malaria-infected mice significantly reduced the activity of serum marker enzymes for liver function like ALT, ALP, and AST (Table 2) and levels of conjugated and unconjugated bilirubin in serum (Fig. 6F). No significant change was noticed in malaria-infected mice, which received normal rabbit serum with respect to malaria-infected mice, which did not receive any serum or antibody (Table 2). Therefore, we conclude that neutrophil depletion significantly prevented liver injury in malaria-infected mice.

**Role of TNF $\alpha$  in Mediating Liver Injury**—Accumulation of free heme in liver may also mediate its cytotoxic effects by sensitizing the hepatocytes to TNF $\alpha$ -mediated apoptosis (23). TNF $\alpha$  also plays a major role in neutrophil infiltration in liver

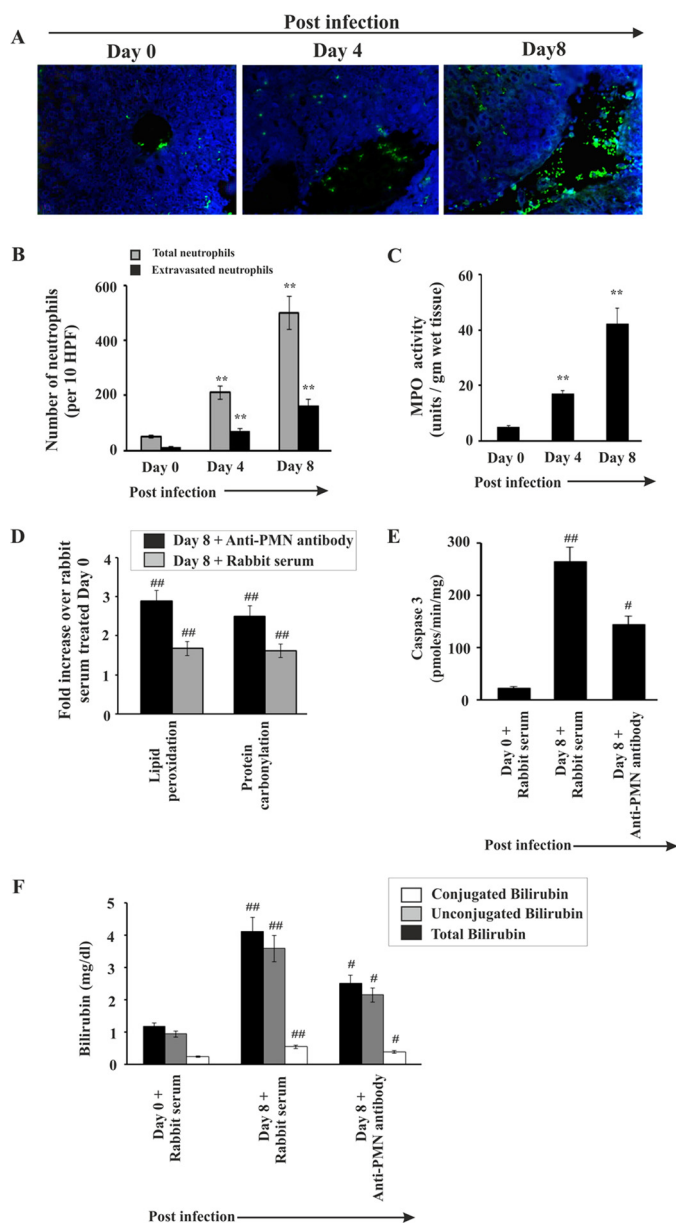


**FIGURE 6. Infiltration of neutrophil in liver during malaria.** *A*, histology of liver showing neutrophil migration. Neutrophils (as indicated by green fluorescence) were detected in infected mice on day 0, 4, and 8 postinfection. *B*, counting of neutrophils in liver sections from different groups of mice. *C*, assay of MPO activity (a marker enzyme for neutrophil) in liver of infected mice on day 0, 4, and 8 postinfection. *D*, fold increase of lipid peroxidation and protein carbonylation in malaria-infected mice on day 8, which received either rabbit serum or anti-PMN antibody from day 3 to 7 postinfection. *E*, measurement of caspase-3 activity in malaria-infected mice on day 0 and day 8 after infection, treated with either normal rabbit serum or anti-PMN antibody. *F*, measurement of bilirubin in malaria-infected mice treated with normal rabbit serum or anti-PMN antibody. Malaria-infected mice on day 0 is considered as control. The details of the methodology are described under "Experimental Procedures." Data are presented as mean  $\pm$  S.E. (\*\*,  $p < 0.01$  versus control; ###,  $p < 0.01$  versus infected mice on day 0 treated with normal rabbit serum; #,  $p < 0.01$  versus infected mice on day 8 treated with normal rabbit serum,  $n = 6$ ).

and other organs (60–62). We were interested to find out the possible role of TNF $\alpha$  in liver injury in malaria. We found a significant increase in TNF $\alpha$  level in the serum of infected mice, which positively correlated with the degree of infection and hemolysis (Fig. 7A). To understand the role of TNF $\alpha$  in liver

injury, we neutralized TNF $\alpha$  by injecting anti-TNF $\alpha$  antibody daily from day 3 to day 7 postinfection. We found that TNF $\alpha$  neutralization resulted in a significant decrease in MPO in the liver as evident from the MPO chlorination assay in liver homogenates indicating significant inhibition of neutrophil infiltration in the liver (Fig. 7B). Subsequently, we measured caspase-3 activity to determine whether or not TNF $\alpha$  neutralization inhibited hepatocyte apoptosis. Data indicated hepatocyte apoptosis was reduced as evident from caspase-3 activity (Fig. 7C). Finally, we assayed AST, ALP, ALT, and bilirubin in the serum of malaria-infected mice after TNF $\alpha$  neutralization to understand the effect of TNF $\alpha$  neutralization on liver injury in malaria. Data indicated significant reduction of the bilirubin level (Fig. 7D) and liver marker enzyme activity in malaria-infected mice after TNF $\alpha$  neutralization (Table 2). Administration of hamster serum in malaria-infected mice (negative control) did not show any significant alteration with respect to malaria-infected mice, which did not receive any serum or antibody (Table 2). Therefore, we conclude that TNF $\alpha$  neutralization prevented neutrophil infiltration in the liver of malaria-infected mice and significantly prevented malaria-induced liver damage.

*Chelation of Iron and Scavenging of Reactive Oxidants Inhibit NF- $\kappa$ B Activation, Expression of Endothelial Cell Adhesion Molecules, Neutrophil Infiltration, and Liver Injury*—Both TNF $\alpha$  and free heme can induce oxidative stress and neutrophil infiltration in liver during malaria. To assess the role of free iron derived from heme and reactive oxidants derived from both heme and TNF $\alpha$  in liver injury, we administered DFO, which is an iron chelator (63), scavenger of reactive oxidants (64), and interacts with heme (65). Furthermore, we also used *N*-acetylcysteine (NAC), which is a scavenger of reactive oxidants and is devoid of iron-chelating or heme-interacting properties. DFO and NAC inhibited NF- $\kappa$ B activation in the liver of infected mice as documented by EMSA (Fig. 8A). The NF- $\kappa$ B-DNA complex formation was significantly reduced in DFO- and NAC-treated mice liver as revealed by EMSA and densitometric analyses (Fig. 8, A and B). Immunoblot of nuclear extracts and densitometric analysis indicated a significant decrease of NF- $\kappa$ B inside the nucleus (Fig. 8, C and D) in DFO- and NAC-treated infected mice. Thus, the data support that free iron and reactive oxidants are responsible for NF- $\kappa$ B activation in liver under severe hemolytic conditions in malaria. ChIP assay was performed to check the binding of NF- $\kappa$ B to the *Icam1* promoter, one of the downstream genes of NF- $\kappa$ B. Chromatin isolated from the liver of DFO- and NAC-treated malaria-infected mice 8 days after infection were immunoprecipitated by anti-NF- $\kappa$ B p65 antibody or rabbit IgG (as negative control). PCR and densitometric analyses showed that the *Icam1* promoter region precipitated by NF- $\kappa$ B p65 antibody was significantly reduced in DFO- and NAC-treated mice. Thus, data revealed that DFO and NAC significantly inhibited the binding of NF- $\kappa$ B to *Icam1* in the liver of malaria-infected mice (Fig. 8, E and F). Furthermore, we performed PCR and densitometric analyses of some of the genes downstream to NF- $\kappa$ B activation like the endothelial cell adhesion molecules *Icam1* and *Vcam1* and the chemokines KC and MIP-2. Data revealed that the expression of these genes was also significantly reduced by DFO and NAC

**TABLE 2**  
**Biochemical analysis of liver function after treatment**

Liver function tests in malaria-infected mice on day 8 postinfection (p.i.) with or without administration of DFO (300 mg/kg) × 2 and NAC (250 mg/kg) mice for 5 consecutive days (3–7 days). The activity of the liver enzymes in serum is expressed in units/liter. Malaria-infected mice on day 0 is considered as control. The details of the methodology are described under “Experimental Procedures.”

Experimental groups	Biochemical analysis of liver function		
	ALT	AST	ALP
	<i>units/liter</i>	<i>units/liter</i>	<i>units/liter</i>
Infected mice on day 0, p.i.	17.16 ± 1.72	44.8 ± 4.5	105.43 ± 11.34
Infected mice on day 8, p.i.	142.4 ± 14.21 <sup>a</sup>	210.82 ± 20.5 <sup>a</sup>	274.97 ± 30.56 <sup>a</sup>
Infected on day 8, p.i. + DFO	69.54 ± 6.96 <sup>b</sup>	108.65 ± 9.56 <sup>b</sup>	157.78 ± 16.12 <sup>b</sup>
Infected on day 8, p.i. + NAC	61.51 ± 6.78 <sup>b</sup>	95.45 ± 9.66 <sup>b</sup>	146.1 ± 13.89 <sup>b</sup>
Infected mice on day 8, p.i. + rabbit serum	139.6 ± 13.88 <sup>c</sup>	214.35 ± 20.5 <sup>c</sup>	272.66 ± 28.89 <sup>c</sup>
Infected mice on day 8, p.i. + anti-PMN antibody	77.76 ± 8.08 <sup>b</sup>	121.94 ± 14.45 <sup>b</sup>	177.93 ± 20.17 <sup>b</sup>
Infected mice on day 8, p.i. + hamster IgG	144.76 ± 4.08 <sup>c</sup>	207.96 ± 20.35 <sup>c</sup>	271.21 ± 27.25 <sup>c</sup>
Infected mice on day 8, p.i. + anti-TNF α antibody	59.41 ± 6.78 <sup>b</sup>	91.32 ± 9.48 <sup>b</sup>	137.81 ± 15.78 <sup>b</sup>

<sup>a</sup> Data were presented as mean ± S.E., *p* < 0.01 versus control.

<sup>b</sup> *p* < 0.01 versus infection on day 8.

<sup>c</sup> *p* < 0.001 versus infection on day 8, *n* = 6.

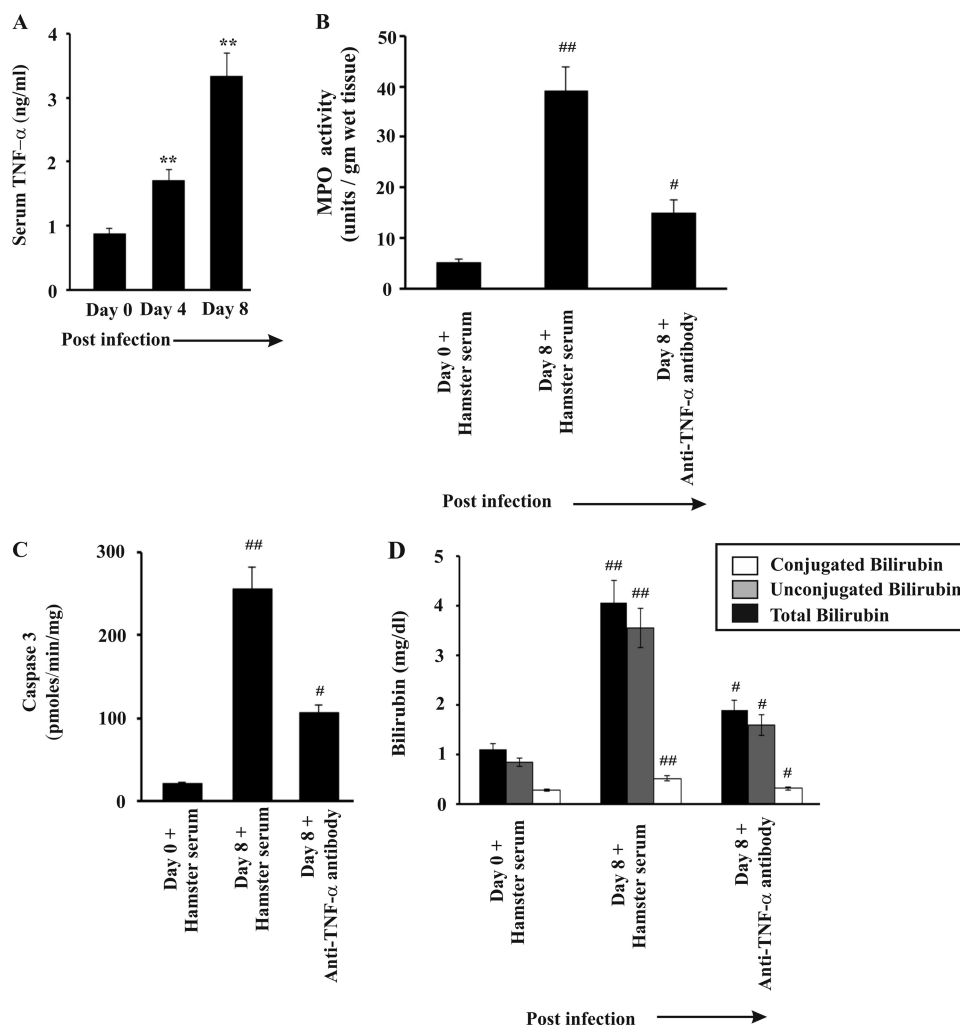


**FIGURE 7. Role of TNF $\alpha$  in liver injury in malaria-infected mice.** *A*, measurement of TNF $\alpha$  in serum of malaria-infected mice on day 0, 4, and 8 postinfection. *B*, assay of MPO activity in liver of infected mice treated with normal hamster serum or anti-TNF $\alpha$  antibody from day 3 to 7 postinfection. *C*, measurement of caspase-3 activity in malaria-infected mice treated with normal hamster serum or anti-TNF $\alpha$  antibody. *D*, measurement of bilirubin in malaria-infected mice treated with normal hamster serum or anti-TNF $\alpha$  antibody. Malaria-infected mice on day 0 is considered as control. The details of the methodology are described under “Experimental Procedures.” Data are presented as mean ± S.E. (\*\*, *p* < 0.01 versus control; ##, *p* < 0.01 versus infected mice on day 0 treated with normal hamster serum; #, *p* < 0.01 versus infected mice on day 8 treated with normal hamster serum, *n* = 6).

(Fig. 9A). Results of immunofluorescence studies confirmed that administration of DFO and NAC in infected mice significantly inhibited neutrophil extravasation in liver as evident from neutrophil count (Fig. 9B). To confirm our results, we

performed MPO chlorination assay of the liver samples obtained after treatment with DFO and NAC and found that there was a significant inhibition in MPO activity (Fig. 9C). Therefore, we conclude that free iron and reactive oxidants

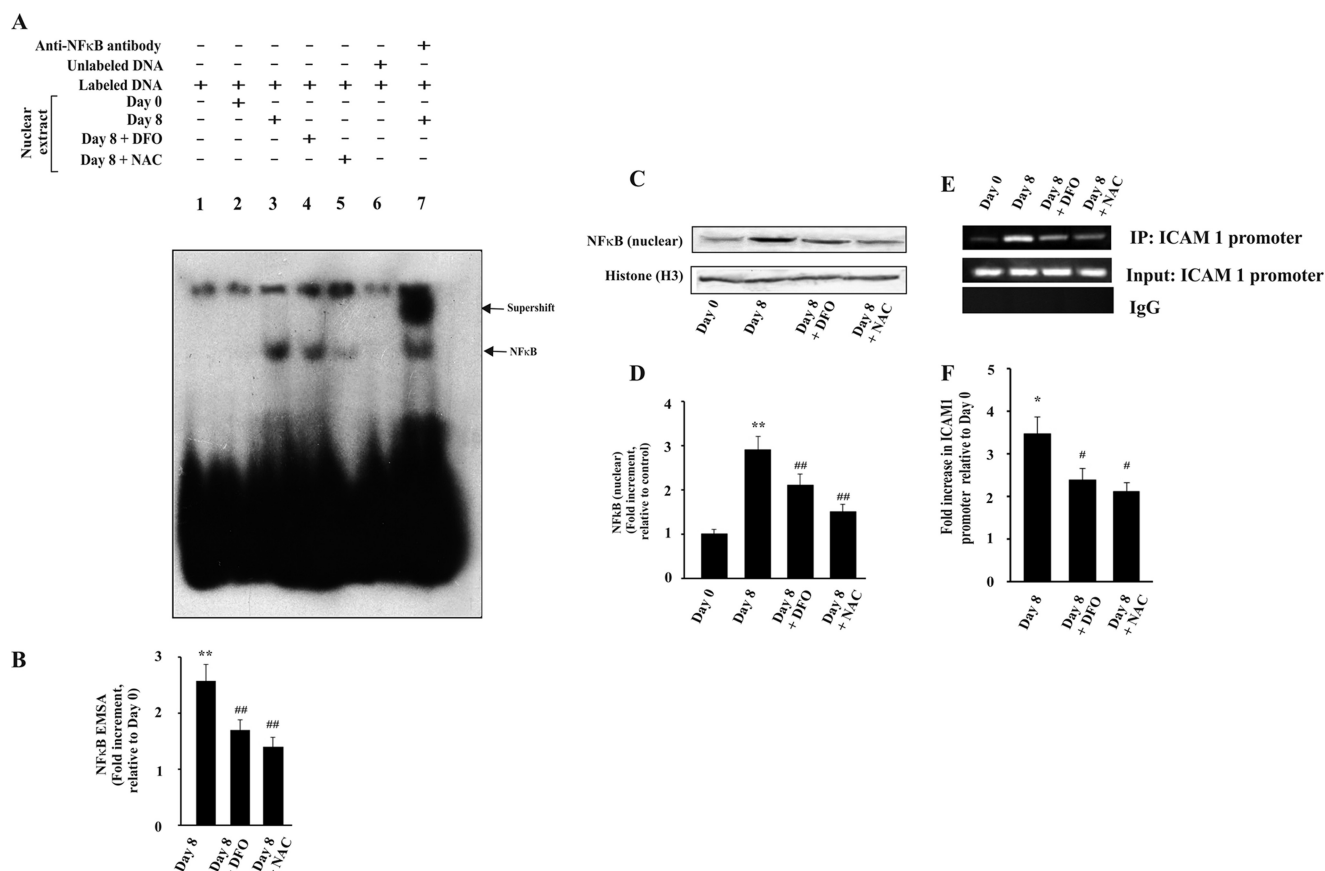


**FIGURE 8. Effect of DFO and NAC on the activation of NF-κB in liver of malaria-infected mice.** *A*, translocation of NF-κB to nucleus as documented by EMSA. Lane 1, only labeled probe and no nuclear extract; lane 2, nuclear extract of liver from mice at day 0 postinfection with labeled probe; lane 3, nuclear extract of liver from infected mice on day 8 postinfection with labeled probe; lane 4, nuclear extract of liver from infected mice on day 8 postinfection and treated with DFO with labeled probe; lane 5, nuclear extract of liver from infected mice on day 8 postinfection and treated with NAC with labeled probe; lane 6, nuclear extract of liver from infected mice on day 8 postinfection with labeled probe and competition with 100-fold excess of cold probe; lane 7, supershift reaction with an antibody specific for NF-κB and nuclear extract of liver from infected mice on day 8 postinfection. *B*, densitometric analysis of EMSA. *C*, detection of NF-κB in nuclear extract from liver of different groups of infected and treated mice by Western immunoblot. *D*, densitometric analysis of Western immunoblot after normalization with the levels of histone H3. *E*, ChIP analysis to follow the recruitment of NF-κB at *Icam1* promoter after treatment with DFO and NAC. *F*, densitometric analysis of ChIP. Malaria-infected mice on day 0 is considered as control. The details of the methodology are described under "Experimental Procedures." Data are presented as mean  $\pm$  S.E. (\*,  $p < 0.1$  versus control; \*\*,  $p < 0.01$  versus control; #,  $p < 0.1$  versus infected at day 8; ##,  $p < 0.01$  versus infected at day 8,  $n = 6$ ).

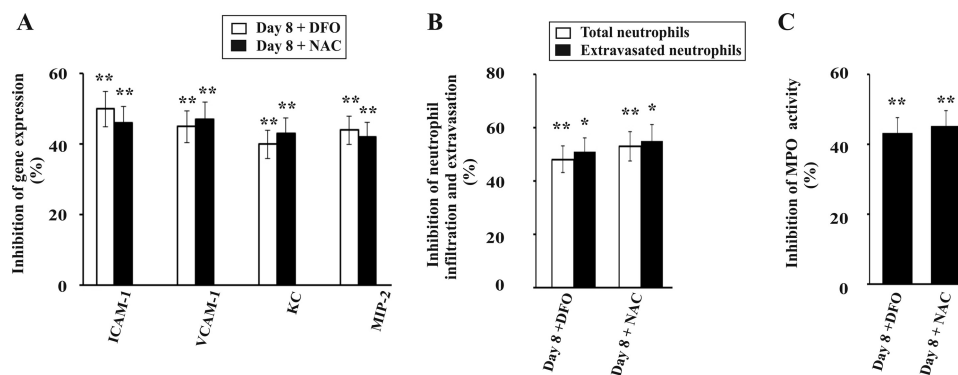


**FIGURE 9. Effect of DFO and NAC on the expression of endothelial cell adhesion molecules, chemokines, and neutrophil infiltration during the infection.** *A*, reduction in expression of *Icam1*, *Vcam1*, *Cxcl1* (KC), and *Cxcl2* (MIP-2) in liver of infected mice on day 8 after treatment with DFO and NAC calculated from densitometric analyses of PCR products of the genes. *B*, inhibition of neutrophil infiltration in liver of infected mice on day 8 after treatment with DFO and NAC as analyzed through immunofluorescence studies by neutrophil count. *C*, inhibition of MPO activity as determined through MPO chlorination assay of infected mice on day 8 after treatment with DFO and NAC. The details of the methodology are described under "Experimental Procedures." Data are presented as mean  $\pm$  S.E. (\*,  $p < 0.1$  versus infected at day 8; \*\*,  $p < 0.01$  versus infected at day 8,  $n = 6$ ).

produced due to hemolysis in malaria are responsible for neutrophil infiltration and extravasation in liver.

Finally, we were interested to see the effect of DFO and NAC on liver dysfunction under hemolytic conditions in malaria.

Both DFO and NAC reduced the generation of reactive oxidants in liver, as revealed by decrease in DCFDA-positive cells. We found that DFO and NAC also significantly prevented oxidative stress as measured by lipid peroxidation and protein car-

## Intravascular Hemolysis and Liver Damage

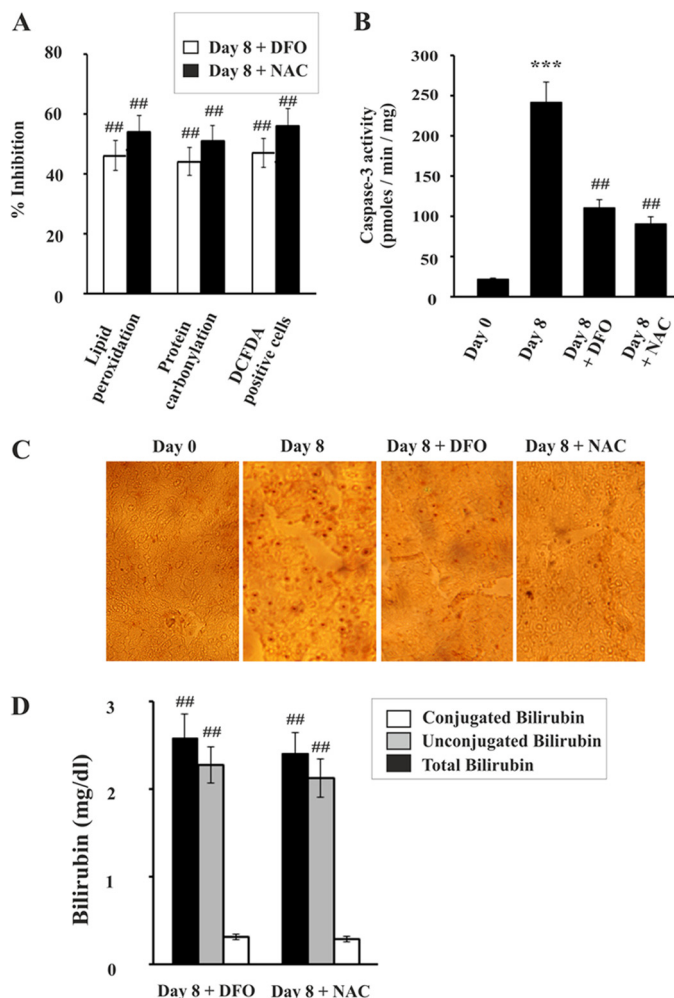


**FIGURE 10. Effect of DFO and NAC on oxidative stress, apoptosis, and liver injury in malaria-infected mice.** *A*, inhibition of protein carbonylation and lipid peroxidation in liver and reactive oxidant generation in hepatocyte by DFO and NAC. *B*, caspase-3 activity assay in liver homogenate of infected mice on day 8 after treatment with DFO and NAC. *C*, TUNEL analysis in liver of infected mice on day 8 after treatment with DFO and NAC. *D*, assay of total, unconjugated, and conjugated bilirubin in serum of infected mice on day 8 after treatment with DFO and NAC. Malaria-infected mice on day 0 is considered as control. The details of the methodology are described under "Experimental Procedures." Data are presented as mean  $\pm$  S.E. (\*\*\*,  $p < 0.001$  versus control; ##,  $p < 0.01$  versus infected at day 8,  $n = 6$ ).

bonylation in the liver of infected mice (Fig. 10A). Reactive oxidants have been reported to be the cause of apoptosis to damage liver (35, 36). DFO and NAC significantly prevented apoptosis in infected mice as evident from the inhibition of caspase-3 activity (Fig. 10B) and the decrease in the number of TUNEL-positive cells (Fig. 10C). Finally, to investigate whether DFO and NAC could protect liver from damage in malaria, we measured bilirubin levels in serum after treatment with DFO and NAC. Data indicated that both DFO and NAC significantly prevented liver injury as evident from reduced levels of conjugated bilirubin (Fig. 10D). The activity of ALT, AST, and ALP levels in serum was also significantly reduced in DFO- and NAC-treated mice (Table 2). Therefore, data confirmed that both DFO and NAC protected the liver under conditions of persistent hemolysis.

## DISCUSSION

We have presented evidence to support a positive correlation between intravascular hemolysis and liver damage using malaria as a model where hemolysis is prevalent. The data indicate that under hemolytic conditions, the overload of heme in liver leads to oxidative stress, which promotes neutrophil infiltration and extravasation in liver through activation of NF- $\kappa$ B, which further aggravates liver damage through the generation of exogenous reactive oxidants. Thus, a vicious cycle of reactive oxidant generation is created to damage liver.

Rodent malaria is an excellent model to explore the impact of persistent hemolysis on organ dysfunction, particularly highly vascular liver (23). Malaria infection-induced liver injury has been reported by many workers (23, 35, 66–69), but the reason is not clear. It is clear that the erythrocytic stage of the life cycle is mainly responsible for hepatopathy or host pathology (23, 35, 66–69). We have inoculated mice with malaria parasite (*P. yoelii*)-infected mouse RBCs (erythrocytic phase) to develop infection. Because the erythrocytic stage of the malaria parasite cannot infect the hepatocytes, it is reasonable to assume that the effect, if any, on liver is not due to parasite invasion to hepatocytes but is due to the toxic products or factors released in blood as result of parasite infection (30, 31, 35). Earlier reports suggest that liver damage occurs in malaria-infected mice due to oxidative stress-mediated apoptosis (23, 35, 36). However, the correlation between hemolysis and liver damage, if any, is not yet established. Our work was targeted to explore the link between hemolysis and liver damage using malaria as a model.

We found severe hemolysis in our model of malaria-infected mice, which subsequently led to heme overload in liver and induced HO-1 and ferritin overexpression. The data indicate that under severe and persistent hemolysis, HO-1 failed to act on all the free heme causing heme overload in liver. HO-1 acts on heme to produce free iron [Fe(II)], which is also a pro-oxidant as it can act as a source of hydroxyl radical ( $\cdot$ OH). Although iron may be sequestered by ferritin, ferritin may not be able to counter the immediate oxidative stress. Malaria infection also causes an increase in TNF $\alpha$  in serum. Heme also sensitizes cells to undergo TNF $\alpha$ -mediated cell death through oxidative stress (23). Therefore, we hypothesize that heme overload in liver is the cause of tremendous reactive oxidant generation in the liver under conditions of severe and persistent hemolysis through Fe(II)-mediated reactions and through synergistic action with TNF $\alpha$ .

Reactive oxidants can regulate NF- $\kappa$ B in a number of ways (70), and reactive oxidant-induced NF- $\kappa$ B activation is well documented (71–73). The mechanism of reactive oxidant-induced NF- $\kappa$ B is also elusive (70, 74). Although NF- $\kappa$ B has been shown to have an anti-apoptotic effect, it can also be pro-apoptotic under certain conditions (75). TNF $\alpha$  can also stimulate NF- $\kappa$ B activation (76). NF- $\kappa$ B regulates the expression of a wide array of genes required for various cellular processes such as inflammation, immunity, cell proliferation, and apoptosis (57, 58). Inappropriate regulation of immune and inflammation cascades causes severe liver injury (77, 78). Therefore, we were interested to find out the response of NF- $\kappa$ B in liver under conditions of acute hemolysis. We found a signification

increase in NF- $\kappa$ B activation in malaria, which is increased with hemolysis. NF- $\kappa$ B signaling is very much related to neutrophil infiltration and inflammation in many diseases (79–81). We further explored whether activation of NF- $\kappa$ B can cause neutrophil activation in liver under hemolytic conditions.

Activation of NF- $\kappa$ B enhances the expression of CXC chemokines in the hepatocytes like KC and MIP-2. These together with other inflammatory mediators can increase the expression of  $\beta_2$  integrins like CD11b/CD18 and many receptors on the surface of the neutrophils (82). Furthermore, they also activate the machinery for generation of reactive oxidants in the neutrophils (82). However, this is not enough to cause damage to the liver (82). Neutrophil extravasation in the liver parenchyma from the hepatic microvasculature is essential for liver injury (82). We observed extravasation of neutrophils in the liver of malaria-infected mice. This can be accredited to both enhanced reactive oxidant generation and production of chemokines in apoptotic and necrotic liver cells. Data from neutrophil migration assay suggested that the ability to attract neutrophils by malaria-infected liver increases with time of infection. The observed chemotactic changes in the liver homogenate, obtained after an extensive perfusion, may be due to many factors. The increased levels of chemokines due to oxidative stress-mediated NF- $\kappa$ B activation in the liver are one of the reasons. Heme has been shown to induce neutrophil chemotaxis (34). Hemozoin is also pro-inflammatory in nature (83, 84). We propose that heme and chemokines in the liver homogenate of malaria-infected mice act as major chemoattractants for neutrophil. However, we cannot ignore the possibility of proteins of parasite origin (antigens) to act as chemoattractants. Although intra-erythrocytic stages of parasites do not infect the hepatocytes, they may exist in the blood vessels of liver. We have perfused the liver, and therefore the parasites in the blood were completely removed. However, there may be a possibility of the presence of proteins, which are secreted by the parasite that may enter the liver and act as chemoattractants.

Once the neutrophils enter liver parenchyma,  $\beta_2$  integrins interact with adhesion molecules like *Icam1* and *Vcam1* on the hepatocytes resulting in adhesion of neutrophils to the hepatocytes. The expression of *Icam1* and *Vcam1* are also induced by activated NF- $\kappa$ B by binding to the promoter of these genes. Adhesion of neutrophils to hepatocytes triggers the generation of tremendous amount of reactive oxidants. Neutrophil adhesion assay confirmed that hepatocytes isolated from malaria-infected liver cells on day 8 can allow adherence of higher number of neutrophils compared with the infected liver cells on day 0. NADPH oxidase in activated neutrophils generates superoxide, which is dismutated to oxygen and hydrogen peroxide. MPO released from the azurophilic granules of neutrophils generates hypochlorous acid from  $H_2O_2$  and chloride ions ( $Cl^-$ ) during respiratory burst of neutrophils. The subsequent products formed are chlorine, chloramines, hydroxyl radicals, singlet oxygen, and ozone that can damage cellular targets *in vivo* (85, 86). Other than these oxidants, neutrophils also produce serine proteases like neutrophil proteinase-3 and elastase, which further aggravate hepatocyte damage (87). Our results suggested an association of NF- $\kappa$ B, oxidative stress, and neutrophil infiltration in liver in the form of a vicious cycle under

hemolytic conditions. Thus, it is clear that persistent hemolysis leads to continuous supply of free heme, which is very toxic to major organs. Liver consists of 60–65% hepatocytes (parenchymal cells) by number. Hepatocytes make up to 70–80% of total cytoplasmic mass of liver (88). The rest are nonparenchymal cells. The changes in NF- $\kappa$ B signaling certainly occur in hepatocytes of malaria-infected mice but may also take place in nonparenchymal cells or infiltrating phagocytes.

To confirm that free iron and reactive oxidants derived from free heme play a major role in liver damage during malaria, we used a heme-interacting iron chelator and a reactive oxidants scavenger. If free iron (derived from heme) and reactive oxidants are the main causes of oxidative stress, NF- $\kappa$ B activation, and neutrophil infiltration in liver, then administration of a heme-interacting iron chelator and reactive oxidants scavenger would reduce these events and protect the liver under conditions of severe hemolysis. The data suggested that reactive oxidants scavenger and iron chelator (DFO) and the antioxidant (NAC) reduced NF- $\kappa$ B activation in liver, expression of chemokines like KC and MIP2, and expression of endothelial cell adhesion molecules like *Icam1* and *Vcam1*. Furthermore, scavenging of reactive oxidants and chelation of free iron prevented not only oxidative stress but also neutrophil infiltration into liver and therefore effectively prevented liver injury under hemolytic conditions. DFO has heme-interacting, iron-chelating, and radical-scavenging properties (63–65). NAC is not an iron chelator, rather it is an effective free radical scavenger. Although we did not find an increase in iron per mg of liver in infected mice on day 8 with respect to infected mice on day 0, we presume that the immediate participation of Fe(II) in Fenton's reaction leads to the generation of free radicals. Free iron is then sequestered by ferritin and redistributed by hepcidin from the hepatocytes to the liver macrophages and spleen (89). The iron chelator would therefore counter the immediate oxidative stress.

DFO has been used to protect patients from toxic effects of iron overload, especially in cases of thalassemia and transfusion-dependent anemias (90). NAC was chosen over other reactive oxidants scavengers because of its strong efficiency to enter inside cells and less toxicity in comparison with other reactive oxidant scavengers. NAC has been used as a reactive oxidant scavenger *in vivo* (91, 92). Neither DFO nor NAC reduced the parasite burden at the dose used indicating that the hepatoprotective effect of DFO and NAC was not due to any antiparasitic effect. The dose of DFO and NAC was decided on the basis of their efficiencies. Because DFO and NAC significantly prevented inflammation-induced changes in the liver of malaria-infected mice, we can conclude that reactive oxidants play a major role in eliciting inflammatory changes in liver during malaria. However, such inflammatory changes may also be induced simply by parasite infection and other factors.

This led us to propose that both free iron and reactive oxidants, derived from heme, act as triggers for oxidative stress and neutrophil infiltration in liver. Oxidative stress and neutrophil infiltration are linked with each other through NF- $\kappa$ B activation. Other than the use of iron chelator and reactive oxidant scavenger, the use of anti-neutrophil antibody and anti-TNF $\alpha$  antibody can be other options to diminish this cycle of reactive

oxidant generation. Anti-neutrophil antibody may prevent neutrophil infiltration but it would not deter the generation of oxidative stress in liver due to the accumulation of free heme and iron. To protect liver or any major organ damage due to accumulation of free heme and subsequent neutrophil infiltration in malaria, a combination therapy of antimalarial and anti-oxidant-iron chelator is highly recommended. We therefore conclude that under conditions of acute hemolysis, liver can be protected by reactive oxidants scavenger and an iron chelator.

### REFERENCES

- Belcher, J. D., Beckman, J. D., Balla, G., Balla, J., and Vercellotti, G. (2010) Heme degradation and vascular injury. *Antioxid. Redox Signal.* **12**, 233–248
- Kato, G. J., and Taylor, J. G., 6th (2010) Pleiotropic effects of intravascular hemolysis on vascular homeostasis. *Br. J. Haematol.* **148**, 690–701
- Woollard, K. J., Sturgeon, S., Chin-Dusting, J. P., Salem, H. H., and Jackson, S. P. (2009) Erythrocyte hemolysis and hemoglobin oxidation promote ferric chloride-induced vascular injury. *J. Biol. Chem.* **284**, 13110–13118
- Qian, Q., Nath, K. A., Wu, Y., Daoud, T. M., and Sethi, S. (2010) Hemolysis and acute kidney failure. *Am. J. Kidney Dis.* **56**, 780–784
- Yang, F., Haile, D. J., Berger, F. G., Herbert, D. C., Van Beveren, E., and Ghio, A. J. (2003) Haptoglobin reduces lung injury associated with exposure to blood. *Am. J. Physiol. Lung Cell Mol. Physiol.* **284**, L402–L409
- Kato, G. J. (2009) Haptoglobin halts hemoglobin's havoc. *J. Clin. Invest.* **119**, 2140–2142
- Tolosano, E., Fagoonee, S., Hirsch, E., Berger, F. G., Baumann, H., Silengo, L., and Altruda, F. (2002) Enhanced splenomegaly and severe liver inflammation in haptoglobin/hemopexin double-null mice after acute hemolysis. *Blood* **100**, 4201–4208
- Smith, A., and Morgan, W. T. (1981) Hemopexin-mediated transport of heme into isolated rat hepatocytes. *J. Biol. Chem.* **256**, 10902–10909
- Smith, A., and Morgan, W. T. (1984) Hemopexin-mediated heme uptake by liver. Characterization of the interaction of heme-hemopexin with isolated rabbit liver plasma membranes. *J. Biol. Chem.* **259**, 12049–12053
- Pal, C., Kundu, M. K., Bandyopadhyay, U., and Adhikari, S. (2011) Synthesis of novel heme-interacting acridone derivatives to prevent free heme-mediated protein oxidation and degradation. *Bioorg. Med. Chem. Lett.* **21**, 3563–3567
- Pal, C., and Bandyopadhyay, U. (2012) Redox-active antiparasitic drugs. *Antioxid. Redox Signal.* **17**, 555–582
- Buehler, P. W., and D'Agnillo, F. (2010) Toxicological consequences of extracellular hemoglobin. Biochemical and physiological perspectives. *Antioxid. Redox Signal.* **12**, 275–291
- Reeder, B. J., Svistunenko, D. A., Cooper, C. E., and Wilson, M. T. (2004) The radical and redox chemistry of myoglobin and hemoglobin. From *in vitro* studies to human pathology. *Antioxid. Redox Signal.* **6**, 954–966
- Kapralov, A., Vlasova, I. I., Feng, W., Maeda, A., Walson, K., Tyurin, V. A., Huang, Z., Aneja, R. K., Carcillo, J., Bayir, H., and Kagan, V. E. (2009) Peroxidase activity of hemoglobin-haptoglobin complexes. Covalent aggregation and oxidative stress in plasma and macrophages. *J. Biol. Chem.* **284**, 30395–30407
- Kumar, S., and Bandyopadhyay, U. (2005) Free heme toxicity and its detoxification systems in human. *Toxicol. Lett.* **157**, 175–188
- Rother, R. P., Bell, L., Hillmen, P., and Gladwin, M. T. (2005) The clinical sequelae of intravascular hemolysis and extracellular plasma hemoglobin. A novel mechanism of human disease. *JAMA* **293**, 1653–1662
- Jeney, V., Balla, J., Yachie, A., Varga, Z., Vercellotti, G. M., Eaton, J. W., and Balla, G. (2002) Pro-oxidant and cytotoxic effects of circulating heme. *Blood* **100**, 879–887
- Nagababu, E., and Rifkind, J. M. (2004) Heme degradation by reactive oxygen species. *Antioxid. Redox Signal.* **6**, 967–978
- Orino, K., Lehman, L., Tsuji, Y., Ayaki, H., Torti, S. V., and Torti, F. M. (2001) Ferritin and the response to oxidative stress. *Biochem. J.* **357**, 241–247
- Ryter, S. W., and Tyrrell, R. M. (2000) The heme synthesis and degradation pathways. Role in oxidant sensitivity. Heme oxygenase has both pro- and antioxidant properties. *Free Radic. Biol. Med.* **28**, 289–309
- Balla, J., Vercellotti, G. M., Jeney, V., Yachie, A., Varga, Z., Jacob, H. S., Eaton, J. W., and Balla, G. (2007) Heme, heme oxygenase, and ferritin. How the vascular endothelium survives (and dies) in an iron-rich environment. *Antioxid. Redox Signal.* **9**, 2119–2137
- Breman, J. G. (2009) Eradicating malaria. *Sci. Prog.* **92**, 1–38
- Seixas, E., Gozzelino, R., Chora, A., Ferreira, A., Silva, G., Larsen, R., Rebelo, S., Penido, C., Smith, N. R., Coutinho, A., and Soares, M. P. (2009) Heme oxygenase-1 affords protection against noncerebral forms of severe malaria. *Proc. Natl. Acad. Sci. U.S.A.* **106**, 15837–15842
- Larkin, D., de Laat, B., Jenkins, P. V., Bunn, J., Craig, A. G., Terraube, V., Preston, R. J., Donkor, C., Grau, G. E., van Mourik, J. A., and O'Donnell, J. S. (2009) Severe *Plasmodium falciparum* malaria is associated with circulating ultra-large von Willebrand multimers and ADAMTS13 inhibition. *PLoS Pathog.* **5**, e1000349
- Fendel, R., Brandts, C., Rudat, A., Kreidenweiss, A., Steur, C., Appelmann, I., Ruehe, B., Schröder, P., Berdel, W. E., Kreamsner, P. G., and Mordmüller, B. (2010) Hemolysis is associated with low reticulocyte production index and predicts blood transfusion in severe malarial anemia. *PLoS ONE* **5**, e10038
- Haldar, K., Hiller, N. L., van Ooij, C., and Bhattacharjee, S. (2005) *Plasmodium* parasite proteins and the infected erythrocyte. *Trends Parasitol.* **21**, 402–403
- Francis, S. E., Sullivan, D. J., Jr., and Goldberg, D. E. (1997) Hemoglobin metabolism in the malaria parasite *Plasmodium falciparum*. *Annu. Rev. Microbiol.* **51**, 97–123
- Bandyopadhyay, U., and Dey, S. (2011) in *Apicomplexan Parasites* (Becker, K., ed) pp. 205–234, Wiley-VCH Verlag GmbH & Co. KGaA, Weinheim, Germany
- Pamplona, A., Ferreira, A., Balla, J., Jeney, V., Balla, G., Epiphany, S., Chora, A., Rodrigues, C. D., Gregoire, I. P., Cunha-Rodrigues, M., Portugal, S., Soares, M. P., and Mota, M. M. (2007) Heme oxygenase-1 and carbon monoxide suppress the pathogenesis of experimental cerebral malaria. *Nat. Med.* **13**, 703–710
- Buffet, P. A., Safeukui, I., Deplaine, G., Brousse, V., Prendki, V., Thellier, M., Turner, G. D., and Mercereau-Puijalon, O. (2011) The pathogenesis of *Plasmodium falciparum* malaria in humans: insights from splenic physiology. *Blood* **117**, 381–392
- Haldar, K., Murphy, S. C., Milner, D. A., and Taylor, T. E. (2007) Malaria. Mechanisms of erythrocytic infection and pathological correlates of severe disease. *Annu. Rev. Pathol.* **2**, 217–249
- Postma, N. S., Mommers, E. C., Eling, W. M., and Zuidema, J. (1996) Oxidative stress in malaria; implications for prevention and therapy. *Pharm. World Sci.* **18**, 121–129
- Orjih, A. U., Banyal, H. S., Chevli, R., and Fitch, C. D. (1981) Hemin lyses malaria parasites. *Science* **214**, 667–669
- Porto, B. N., Alves, L. S., Fernández, P. L., Dutra, T. P., Figueiredo, R. T., Graça-Souza, A. V., and Bozza, M. T. (2007) Heme induces neutrophil migration and reactive oxygen species generation through signaling pathways characteristic of chemotactic receptors. *J. Biol. Chem.* **282**, 24430–24436
- Guha, M., Kumar, S., Choubey, V., Maity, P., and Bandyopadhyay, U. (2006) Apoptosis in liver during malaria. Role of oxidative stress and implication of mitochondrial pathway. *FASEB J.* **20**, 1224–1226
- Dey, S., Guha, M., Alam, A., Goyal, M., Bindu, S., Pal, C., Maity, P., Mitra, K., and Bandyopadhyay, U. (2009) Malarial infection develops mitochondrial pathology and mitochondrial oxidative stress to promote hepatocyte apoptosis. *Free Radic. Biol. Med.* **46**, 271–281
- Farombi, E. O., Shrotriya, S., Na, H. K., Kim, S. H., and Surh, Y. J. (2008) Curcumin attenuates dimethylnitrosamine-induced liver injury in rats through Nrf2-mediated induction of heme oxygenase-1. *Food Chem. Toxicol.* **46**, 1279–1287
- Bindu, S., Pal, C., Dey, S., Goyal, M., Alam, A., Iqbal, M. S., Dutta, S., Sarkar, S., Kumar, R., Maity, P., and Bandyopadhyay, U. (2011) Translocation of heme oxygenase-1 to mitochondria is a novel cytoprotective mechanism against nonsteroidal anti-inflammatory drug-induced mitochondrial oxidative stress, apoptosis and gastric mucosal injury. *J. Biol. Chem.* **286**,

- 39387–39402
39. Gonçalves, L. A., Vigário, A. M., and Penha-Gonçalves, C. (2007) Improved isolation of murine hepatocytes for *in vitro* malaria liver stage studies. *Malar. J.* **6**, 169
  40. Lowry, O. H., Rosebrough, N. J., Farr, A. L., and Randall, R. J. (1951) Protein measurement with the Folin phenol reagent. *J. Biol. Chem.* **193**, 265–275
  41. Kim, Y. M., de Vera, M. E., Watkins, S. C., and Billiar, T. R. (1997) Nitric oxide protects cultured rat hepatocytes from tumor necrosis factor- $\alpha$ -induced apoptosis by inducing heat shock protein 70 expression. *J. Biol. Chem.* **272**, 1402–1411
  42. Kalyanaraman, B., Darley-Usmar, V., Davies, K. J., Dennery, P. A., Forman, H. J., Grisham, M. B., Mann, G. E., Moore, K., Roberts, L. J., 2nd, and Ischiropoulos, H. (2012) Measuring reactive oxygen and nitrogen species with fluorescent probes. Challenges and limitations. *Free Radic. Biol. Med.* **52**, 1–6
  43. Maity, P., Bindu, S., Dey, S., Goyal, M., Alam, A., Pal, C., Mitra, K., and Bandyopadhyay, U. (2009) Indomethacin, a nonsteroidal anti-inflammatory drug, develops gastropathy by inducing reactive oxygen species-mediated mitochondrial pathology and associated apoptosis in gastric mucosa. A novel role of mitochondrial aconitase oxidation. *J. Biol. Chem.* **284**, 3058–3068
  44. Sajjan, M. P., Standaert, M. L., Nimal, S., Varanasi, U., Pastoor, T., Mastorides, S., Braun, U., Leitges, M., and Farese, R. V. (2009) The critical role of atypical protein kinase C in activating hepatic SREBP-1c and NF- $\kappa$ B in obesity. *J. Lipid Res.* **50**, 1133–1145
  45. Fouad, D., Siendones, E., Costán, G., and Muntané, J. (2004) Role of NF- $\kappa$ B activation and nitric oxide expression during PGE protection against D-galactosamine-induced cell death in cultured rat hepatocytes. *Liver Int.* **24**, 227–236
  46. Russo-Carbolante, E. M., Azzolini, A. E., Polizello, A. C., and Lucisano-Valim, Y. M. (2002) Comparative study of four isolation procedures to obtain rat neutrophils. *Comp. Clin. Pathol.* **11**, 71–76
  47. Wiemer, A. J., Lokuta, M. A., Surfus, J. C., Wernimont, S. A., and Huttenlocher, A. (2010) Calpain inhibition impairs TNF- $\alpha$ -mediated neutrophil adhesion, arrest, and oxidative burst. *Mol. Immunol.* **47**, 894–902
  48. Weiss, S. J., Klein, R., Slivka, A., and Wei, M. (1982) Chlorination of taurine by human neutrophils. Evidence for hypochlorous acid generation. *J. Clin. Invest.* **70**, 598–607
  49. Hao, Q., Chen, Y., Zhu, Y., Fan, Y., Palmer, D., Su, H., Young, W. L., and Yang, G. Y. (2007) Neutrophil depletion decreases VEGF-induced focal angiogenesis in the mature mouse brain. *J. Cereb. Blood Flow Metab.* **27**, 1853–1860
  50. Pal, C., Bindu, S., Dey, S., Alam, A., Goyal, M., Iqbal, M. S., Sarkar, S., Kumar, R., Halder, K. K., Debnath, M. C., Adhikari, S., and Bandyopadhyay, U. (2012) Tryptamine-gallic acid hybrid prevents nonsteroidal anti-inflammatory drug-induced gastropathy. Correction of mitochondrial dysfunction and inhibition of apoptosis in gastric mucosal cells. *J. Biol. Chem.* **287**, 3495–3509
  51. Guha, M., Maity, P., Choubey, V., Mitra, K., Reiter, R. J., and Bandyopadhyay, U. (2007) Melatonin inhibits free radical-mediated mitochondrially dependent hepatocyte apoptosis and liver damage induced during malarial infection. *J. Pineal Res.* **43**, 372–381
  52. Biswas, K., Bandyopadhyay, U., Chattopadhyay, I., Varadaraj, A., Ali, E., and Banerjee, R. K. (2003) A novel antioxidant and antiapoptotic role of omeprazole to block gastric ulcer through scavenging of hydroxyl radical. *J. Biol. Chem.* **278**, 10993–11001
  53. Pal, C., Bindu, S., Dey, S., Alam, A., Goyal, M., Iqbal, M. S., Maity, P., Adhikari, S. S., and Bandyopadhyay, U. (2010) Gallic acid prevents nonsteroidal anti-inflammatory drug-induced gastropathy in rat by blocking oxidative stress and apoptosis. *Free Radic. Biol. Med.* **49**, 258–267
  54. Maity, P., Bindu, S., Dey, S., Goyal, M., Alam, A., Pal, C., Reiter, R., and Bandyopadhyay, U. (2009) Melatonin reduces indomethacin-induced gastric mucosal cell apoptosis by preventing mitochondrial oxidative stress and the activation of mitochondrial pathway of apoptosis. *J. Pineal Res.* **46**, 314–323
  55. Smith, A., and Morgan, W. T. (1985) Hemopexin-mediated heme transport to the liver. Evidence for a heme-binding protein in liver plasma membranes. *J. Biol. Chem.* **260**, 8325–8329
  56. Eskew, J. D., Vanacore, R. M., Sung, L., Morales, P. J., and Smith, A. (1999) Cellular protection mechanisms against extracellular heme. Heme-hemopexin, but not free heme, activates the N-terminal c-Jun kinase. *J. Biol. Chem.* **274**, 638–648
  57. Li, Q., and Verma, I. M. (2002) NF- $\kappa$ B regulation in the immune system. *Nat. Rev. Immunol.* **2**, 725–734
  58. Liang, Y., Zhou, Y., and Shen, P. (2004) NF- $\kappa$ B and its regulation on the immune system. *Cell. Mol. Immunol.* **1**, 343–350
  59. Kabe, Y., Ando, K., Hirao, S., Yoshida, M., and Handa, H. (2005) Redox regulation of NF- $\kappa$ B activation. Distinct redox regulation between the cytoplasm and the nucleus. *Antioxid. Redox Signal.* **7**, 395–403
  60. Bombini, G., Canetti, C., Rocha, F. A., and Cunha, F. Q. (2004) Tumor necrosis factor- $\alpha$  mediates neutrophil migration to the knee synovial cavity during immune inflammation. *Eur. J. Pharmacol.* **496**, 197–204
  61. Lokuta, M. A., and Huttenlocher, A. (2005) TNF- $\alpha$  promotes a stop signal that inhibits neutrophil polarization and migration via a p38 MAPK pathway. *J. Leukocyte Biol.* **78**, 210–219
  62. Perry, B. C., Soltys, D., Toledo, A. H., and Toledo-Pereyra, L. H. (2011) Tumor necrosis factor- $\alpha$  in liver ischemia/reperfusion injury. *J. Invest. Surg.* **24**, 178–188
  63. Kalinowski, D. S., and Richardson, D. R. (2005) The evolution of iron chelators for the treatment of iron overload disease and cancer. *Pharmacol. Rev.* **57**, 547–583
  64. Caraceni, P., Van Thiel, D. H., and Borle, A. B. (1995) Dual effect of deferoxamine on free radical formation and reoxygenation injury in isolated hepatocytes. *Am. J. Physiol.* **269**, G132–G137
  65. Sullivan, S. G., Baysal, E., and Stern, A. (1992) Inhibition of hemin-induced hemolysis by desferrioxamine. Binding of hemin to red cell membranes and the effects of alteration of membrane sulfhydryl groups. *Biochim. Biophys. Acta* **1104**, 38–44
  66. Santos, L. C., Abreu, C. F., Xerinda, S. M., Tavares, M., Lucas, R., and Sarmento, A. C. (2012) Severe imported malaria in an intensive care unit. A review of 59 cases. *Malar. J.* **11**, 96
  67. Haque, A., Best, S. E., Amante, F. H., Ammerdorffer, A., de Labastida, F., Pereira, T., Ramm, G. A., and Engwerda, C. R. (2011) High parasite burdens cause liver damage in mice following *Plasmodium berghei* ANKA infection independently of CD8<sup>+</sup> T cell-mediated immune pathology. *Infect. Immun.* **79**, 1882–1888
  68. Yoshimoto, T., Takahama, Y., Wang, C. R., Yoneto, T., Waki, S., and Nariuchi, H. (1998) A pathogenic role of IL-12 in blood-stage murine malaria lethal strain *Plasmodium berghei* NK65 infection. *J. Immunol.* **160**, 5500–5505
  69. Seixas, E., Oliveira, P., Moura Nunes, J. F., and Coutinho, A. (2008) An experimental model for fatal malaria due to TNF- $\alpha$ -dependent hepatic damage. *Parasitology* **135**, 683–690
  70. Bubicic, C., Papa, S., Dean, K., and Franzoso, G. (2006) Mutual cross-talk between reactive oxygen species and nuclear factor- $\kappa$ B. Molecular basis and biological significance. *Oncogene* **25**, 6731–6748
  71. Schieven, G. L., Kirihara, J. M., Myers, D. E., Ledbetter, J. A., and Uckun, F. M. (1993) Reactive oxygen intermediates activate NF- $\kappa$ B in a tyrosine kinase-dependent mechanism and in combination with vanadate activate the p56lck and p59fyn tyrosine kinases in human lymphocytes. *Blood* **82**, 1212–1220
  72. Schoonbroodt, S., Ferreira, V., Best-Belpomme, M., Boelaert, J. R., Legrand-Poels, S., Korner, M., and Piette, J. (2000) Crucial role of the amino-terminal tyrosine residue 42 and the carboxyl-terminal PEST domain of I $\kappa$ B $\alpha$  in NF- $\kappa$ B activation by an oxidative stress. *J. Immunol.* **164**, 4292–4300
  73. Takada, Y., Mukhopadhyay, A., Kundu, G. C., Mahabeleshwar, G. H., Singh, S., and Aggarwal, B. B. (2003) Hydrogen peroxide activates NF- $\kappa$ B through tyrosine phosphorylation of I $\kappa$ B $\alpha$  and serine phosphorylation of p65. Evidence for the involvement of I $\kappa$ B $\alpha$  kinase and Syk protein-tyrosine kinase. *J. Biol. Chem.* **278**, 24233–24241
  74. Morgan, M. J., and Liu, Z. G. (2011) Cross-talk of reactive oxygen species and NF- $\kappa$ B signaling. *Cell Res.* **21**, 103–115
  75. Perkins, N. D., and Gilmore, T. D. (2006) Good cop, bad cop. The different faces of NF- $\kappa$ B. *Cell Death Differ.* **13**, 759–772

## Intravascular Hemolysis and Liver Damage

76. Baldwin, A. S., Jr. (1996) The NF- $\kappa$ B and I $\kappa$ B proteins. New discoveries and insights. *Annu. Rev. Immunol.* **14**, 649–683
77. Adams, D. H., Ju, C., Ramaiah, S. K., Uetrecht, J., and Jaeschke, H. (2010) Mechanisms of immune-mediated liver injury. *Toxicol. Sci.* **115**, 307–321
78. Dienes, H. P., and Drebber, U. (2010) Pathology of immune-mediated liver injury. *Dig. Dis.* **28**, 57–62
79. Tak, P. P., and Firestein, G. S. (2001) NF- $\kappa$ B. A key role in inflammatory diseases. *J. Clin. Invest.* **107**, 7–11
80. Nanji, A. A., Jokelainen, K., Rahemtulla, A., Miao, L., Fogt, F., Matsumoto, H., Tahan, S. R., and Su, G. L. (1999) Activation of nuclear factor  $\kappa$ B and cytokine imbalance in experimental alcoholic liver disease in the rat. *Hepatology* **30**, 934–943
81. McDonald, B., and Kubes, P. (2012) Neutrophils and intravascular immunity in the liver during infection and sterile inflammation. *Toxicol. Pathol.* **40**, 157–165
82. Jaeschke, H. (2006) Mechanisms of liver injury. II. Mechanisms of neutrophil-induced liver cell injury during hepatic ischemia-reperfusion and other acute inflammatory conditions. *Am. J. Physiol. Gastrointest. Liver Physiol.* **290**, G1083–L1088
83. Jaramillo, M., Plante, I., Ouellet, N., Vandal, K., Tessier, P. A., and Olivier, M. (2004) Hemozoin-inducible proinflammatory events *in vivo*. Potential role in malaria infection. *J. Immunol.* **172**, 3101–3110
84. Griffith, J. W., Sun, T., McIntosh, M. T., and Bucala, R. (2009) Pure Hemozoin is inflammatory *in vivo* and activates the NALP3 inflammasome via release of uric acid. *J. Immunol.* **183**, 5208–5220
85. Klebanoff, S. J. (2005) Myeloperoxidase. Friend and foe. *J. Leukocyte Biol.* **77**, 598–625
86. Vasilyev, N., Williams, T., Brennan, M. L., Unzek, S., Zhou, X., Heinecke, J. W., Spitz, D. R., Topol, E. J., Hazen, S. L., and Penn, M. S. (2005) Myeloperoxidase-generated oxidants modulate left ventricular remodeling but not infarct size after myocardial infarction. *Circulation* **112**, 2812–2820
87. Shimakura, A., Kamanaka, Y., Ikeda, Y., Kondo, K., Suzuki, Y., and Umemura, K. (2000) Neutrophil elastase inhibition reduces cerebral ischemic damage in the middle cerebral artery occlusion. *Brain Res.* **858**, 55–60
88. Ramadori, G., Moriconi, F., Malik, I., and Dudas, J. (2008) Physiology and pathophysiology of liver inflammation, damage, and repair. *J. Physiol. Pharmacol.* **59**, 107–117
89. Portugal, S., Carret, C., Recker, M., Armitage, A. E., Gonçalves, L. A., Epiphany, S., Sullivan, D., Roy, C., Newbold, C. I., Drakesmith, H., and Mota, M. M. (2011) Host-mediated regulation of superinfection in malaria. *Nat. Med.* **17**, 732–737
90. Cianciulli, P. (2009) Iron chelation therapy in thalassemia syndromes. *Mediterr. J. Hematol. Infect. Dis.* **1**, e2009034
91. Sathish, P., Paramasivan, V., Palani, V., and Sivanesan, K. (2011) *N*-Acetylcysteine attenuates dimethylnitrosamine-induced oxidative stress in rats. *Eur. J. Pharmacol.* **654**, 181–186
92. Baniyadi, S., Eftekhari, P., Tabarsi, P., Fahimi, F., Raoufy, M. R., Masjedi, M. R., and Velayati, A. A. (2010) Protective effect of *N*-acetylcysteine on antituberculosis drug-induced hepatotoxicity. *Eur. J. Gastroenterol. Hepatol.* **22**, 1235–1238

**Impact of Intravascular Hemolysis in Malaria on Liver Dysfunction:  
INVOLVEMENT OF HEPATIC FREE HEME OVERLOAD, NF-  $\kappa$ B  
ACTIVATION, AND NEUTROPHIL INFILTRATION**

Sumanta Dey, Samik Bindu, Manish Goyal, Chinmay Pal, Athar Alam, Mohd. Shameel  
Iqbal, Rahul Kumar, Souvik Sarkar and Uday Bandyopadhyay

*J. Biol. Chem.* 2012, 287:26630-26646.

doi: 10.1074/jbc.M112.341255 originally published online June 13, 2012

---

Access the most updated version of this article at doi: [10.1074/jbc.M112.341255](https://doi.org/10.1074/jbc.M112.341255)

Alerts:

- [When this article is cited](#)
- [When a correction for this article is posted](#)

[Click here](#) to choose from all of JBC's e-mail alerts

This article cites 91 references, 36 of which can be accessed free at  
<http://www.jbc.org/content/287/32/26630.full.html#ref-list-1>